Numerical analysis of vacuum drying of a porous body in the integrated domain

Running Title: **vacuum drying of a porous body**

Milad Amiri [1, 2], Mohammad bagher Ayani [2*], Pawel Ziolkowski[1], Dariusz Mikielewicz[1]

[1] Faculty of Mechanical Engineering and Ship Technology, Gdansk University of Technology, Poland

[2] Department of Mechanical Engineering, Ferdowsi university of Mashhad, Iran

[*] Corresponding author. Tel.: +989155117671; fax: +985118763304
 E-mail address: mbayani@um.ac.ir

ORCID iD:

Milad Amiri: https://orcid.org/0000-0002-7794-6297

Mohamad bagher Ayani: https://orcid.org/0000-0002-6874-9603

Pawel Ziolkowski: https://orcid.org/0000-0001-7480-0420

Dariusz Mikielewicz: https://orcid.org/0000-0001-8267-7194

Numerical analysis of vacuum drying of a porous body in the integrated domain

Abstract

In the present study, the vacuum drying process of an apple slice is numerically modeled based on a control volume method. Transient two-dimensional Navier- Stokes, energy, moisture and Luikov equations are solved by numerical coding (Fortran) to simulate the simultaneous heat and mass transfer in the ambient and apple slice respectively. The privilege of using Luikov's model is that the capillary forces are considered, and a differentiation between air, vapor, liquid, and solid is made. Luikov described the two phenomena associated with the transport of air, vapor and liquids through the porous media as molecular transport and molar transport. The ambient pressure linearly reduced within a minute until it reached a constant value. One of the intellectually demanding preoccupations among researchers is how to simulate the sample and its surroundings with high accuracy of boundary conditions which enables to avoid the use of empirical transfer coefficients. This study can be scrutinized from various dimensions, among which non-use of boundary condition between a porous sample and its surroundings is the most conspicuous novelty. Results showed that although at 50 second, isothermal and iso-moisture lines inside the sample are symmetric, they are not symmetric at 100, 200 and 400 second. In addition, at first minute, pump operation leads to vary the density of the Isothermal and Iso-moisture lines around the sample, but at 100, 200 and 400 second higher temperature and moisture gradients have been achieved at the right and top of the sample surface.

Keywords

Capillary-Porous Sample; Heat and Mass Transfer; Luikov equations; Fortran

1. Introduction

Drying has been the way of food preserving since the beginning of the time. Naturally, food, in general, begins to decay and eventually spoil as soon as it is being collected or harvested, when our ancestors found the ways to preserve the food, they could put down root and live in one place rather than migrating in order to harness the nature. Drying inhibits the growth of bacteria, yeasts, and mold through the removal of water (Nummer, 2002). In time, the drying techniques became more and more specialized, and so like many other technical aspects of human life, engineering began to intervene in order to idealize the process in mathematical terms. There are numerous drying techniques offered to dehydrate different kinds of raw materials in order to obtain products of a high-quality conjugate on processing parameters (Si et al., 2016). However, reduction of the nutritional value and the development of undesirable colors, flavors, and textures are observed in oil-fried or hot air–dried fruit and vegetable products (Yongsawatdigul and Gunasekaran, 1996). These characteristics are probably due to processing deficiencies such as excessively high

temperature, long drying time, and inefficient application of energy. The increasing need for producing efficiently high quality and convenient products at a lower cost has led to the use of several drying methods in practice (Karathanos and Saravacos, 1993; Kostaropoulos and Saravacos, 1995; Saravacos, 1967). Due to a significant reduction in the drying time and a relatively good quality of dehydrated product with high energy efficiency, vacuum drying is considered a more advanced and cost-efficient method of drying.

Nomenclature			
A_{cell}	area of the sample (m^2)	S_p	source term
a_e	eastern coefficient of the discretized equation	T	temperature (^0C)
a_f	coefficient of filtration diffusion	t	Time (s)
a_{m1}^T	thermal diffusion coefficient of a moist body	u_p	flow velocity in the direction of central node ($m.s^{-1}$)
a_n	north coefficient of the discretized equation	$\mathbf{v}$	velocity (m s^{-1})
a_s	south coefficient of the discretized equation	v_k	specific volume
a_w	Western coefficient of the discretized equation	v_p	the velocity perpendicular to the direction of flow of central node ($m.s^{-1}$)
$\mathbf{b}$	mass force of Earth gravity (m s^{-2})	*Subscript*	
c	species concentration for mass transfer	0	initial
C_f	body capacity for the humid air with filtration	a	dry air
c_m	mass capacity ($1.^0M^{-1}$)	d	dry
c_q	heat capacity (J.kg^{-1}K^{-1})	v	water vapor
c_v	specific heat capacity at the constant volume	*Greek symbols*	
D	mass diffusivity	ε	penetration of the moisture vapor permeability coefficient
e	specific energy	λ	latent heat of vaporization (J.kg^{-1})
F_{shear}	shear force (N)	ρ	density of air

$\mathbf{j}_k$	density of a mass flow of the kth component of a bound substance in the state k	σ	thermal conductivity (Wm^{-1} K^{-1}).
k_f	thermal conductivity coefficient of the environment	θ	body moisture potential (^{0}M)
k_{fc}	total filtration-coefficient.	δ	coefficient of thermal gradient (K.m^{-1})
k_m	mass diffusivity (kg.m^{-1}.s^{-1}.^{0}M^{-1})	$\emptyset$	moisture content
k_q	thermal conductivity (W.m^{-1}.K^{-1})	ρ_0	density of moist body
p	thermodynamical pressure (Pa)	$\emptyset_k$	relative concentration of the bound body
$\mathbf{q}$	heat flux	τ_{wall}	shear stress ($N.m^{-2}$)
S_c	source of species	μ	dynamic viscosity ($kg.m^{-1}.s^{-1}$)
S_e	source of energy	ω	concentration
S_k	mass source or sink of the kth component		
S_m	source of mass		

Also Si et al. (2016) suggested vacuum microwave drying was found to present the better quality of raspberry powders among the thermal drying techniques. The drying process is performed in different ways such as vacuum drying (Šumić, Tepić, Vidović, Jokić, and Malbaša, 2013), freeze-drying (Carullo and Vallan, 2012), solar drying (Sontakke and Salve, 2015), spray drying (Shi, Li, Wang, Zhou, and Adhikari, 2012), and convective drying (Mohan and Talukdar, 2010). In vacuum drying, the vacuum is often applied as a process to remove water and other solvents that have been absorbed by surface and body volume. In this way, those materials that are sensitive to high temperature can be adequately dried in a short time. Additionally, vacuum drying is capable of preventing the oxidation of the air oxidation sensitive material. Moreover, the process of vacuum drying can also recover removed solvents from the material if it is necessary. The process of vacuum drying has been studied through analytical, experimental, and numerical methods. Fohr et al. (1995) have provided a model for continuous vacuum dryer with hot plates that can keep the temperature of the drying body surface above the boiling point of water. Suvarnakuta et al. (2007) and Swasdisevi et al. (2009) have provided a liquid diffusion model for drying under low pressure. Abbasi (2017) have developed a method in order to dry and powder yogurt leading to increase its shelf life and functional capabilities. The proposed method for studying the process of vacuum drying by Erriguible et al. (2007) consists of solving conservation equations in both porous material and surrounding liquid domains and subsequently linking variables of two domains via boundary conditions.

Heat and mas transfer between capillary-porous bodies and surrounding accompanied by a change of phase is not only of theoretical interest (Badur, Feidt, and Ziółkowski, 2020; Gawin, Pesavento, and Schrefler, 2006; Nowacki, 1974; Wachowicz-Pyzik, Sowiżdżał, Pająk, Ziółkowski, and Badur, 2020; Ziółkowski and Badur, 2018) but also of great practical importance for some technological processes. Phase changes (evaporation of a liquid) essentially influence the intensity of heat and mass transfer between a body surface and the surrounding medium (external heat and mass transfer). Heat and mass transfer inside a porous body (internal heat and mass transfer) also has its unique character (Incropera, Lavine, Bergman, and DeWitt, 2007). Transfer of noncondensing gases, vapor, and liquid may occur in a capillary-porous body. Transfer of vapor and inert gas proceeds in different ways: by diffusion and effusion (molecular transport) and by filtration under the pressure gradient (molar transport). Transport of a liquid occurs by diffusion, capillary absorption, and by filtration. Consequently, the derivation of mass-transfer relations in capillary-porous bodies (Kojic et al., 2017; Yang, Li, and Sun, 2020) on the basis of a molecular and molar transport mechanism involves great difficulties. Physical characterization and mass modeling of dried Terminalia chebula fruit was investigated by Pathak et al. (2019) in a porous media. The value of porosity for the fruit was considered to be $79.23 \pm 0.09\%$ required in heat flow and airflow studies. The linear and quadratic models illustrated the best relations between the dimensional and mass parameters of the fruit. The experimental analysis of specific energy consumption, drying kinetics and microstructural changes of sweet potato was studied by Onwude et al. (2018). Infrared drying, convective hot-air drying and combine of them have been used and results showed a more porous microstructure of sweet potato in using combined modelling. In addition, Increased porosity occurred at higher model heat flux results in increased internal stress and water evaporation in the cells. Nalawade et al. (2018) investigated combination of infrared and hybrid drying consisting of infrared -hot air for bitter gourd slices. The results indicated that higher moisture diffusivity and rehydration ratio in combination method leads to porous structure of slices. Combined heat pump drying with freeze-drying of Antarctic krill and its effects on the lipids in a porous media was investigated by Sun et al. (2017). The results demonstrated that the sample after combination treatment by heat pump drying and freeze-drying had more microporous than either of freeze-drying and heat pump drying alone, respectively, which could be due to the sublimation of moisture.

In the present study the vacuum drying process is analyzed using a two-dimensional transient numerical heat and mass transfer of an apple in a quadrate geometry based on a control volume method. The lack of previous modeling about the internal geometry of the porous medium especially in the corners of the sample made us to simulate sample and it's ambient, so that it is to be able to show behaviors of all points sample and vacuum chamber accurately. In addition, previous researchers used boundary conditions with using empirical transfer coefficients, which, in turn, decrease the accuracy of surrounding conditions of sample (Amiri and Ayani, 2014; Andarwa and Tabrizi, 2010; Chang and Weng, 2000; Kocaefe, Younsi, Poncsak, and Kocaefe, 2007; Rani and Tripathy, 2020; Younsi, Kocaefe, Poncsak, and Kocaefe, 2007), but, in this work, for the first time, the vacuum drying integrated simulation with non-use of boundary condition between sample and its

ambient is achieved simultaneously to simulate the heat and mass transfer in the ambient and the apple slice.

2. Modeling

In vacuum drying, the vacuum pump eliminated the air inside the chamber and then drying operation takes place at a constant pressure. In the other word, transient flow regime results from changes on the operational conditions (Boye and Samuel, 2020). The geometry of the square sample in the vacuum chamber is shown in Figure.1. It is assumed that the square sample is placed in the center of the vacuum chamber. The chamber pressure decreased linearly from 101325 to 20000 Pa in 1 min (see Figure.1); then is kept constant. The isothermal walls of the chamber, whose temperature is fixed at 60°C, causes to prevent the reduction of sample surface temperature, due to the gas expansion in the chamber. The temperature of chamber walls is low enough to ignore the effect of thermal radiation. The initial temperature and moisture potential of air are 60 °C and 12(°M) respectively and assumed to be uniform.

$$P(t) = \begin{cases} 101325 - 1400\,t \text{ (Pa)} & \text{if } 0 < t < 58s \\ 20000 \text{ (Pa)} & \text{if } t \geq 58s \end{cases}$$
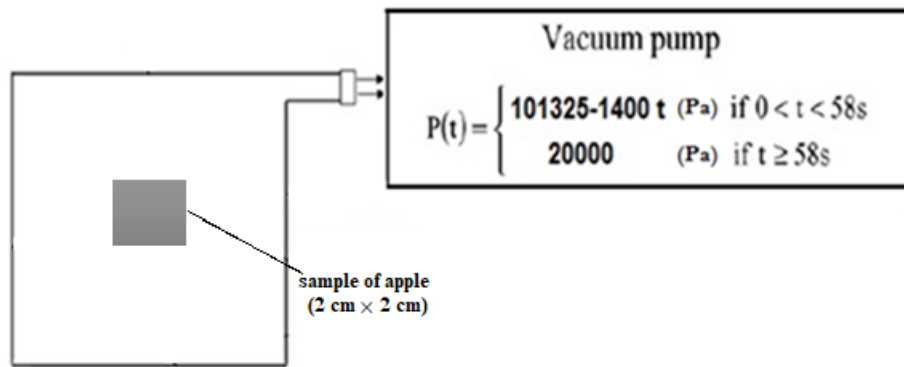
sample of apple
(2 cm × 2 cm)

Figure 1. The schematic of the vacuum chamber and the sample

2.1. Modelling for the space of chamber

The physical analysis is carried out by dividing the drying process in two periods. During the first one, there is an air flow. The flow of moist air is considered as a mixture of ideal gas. The simplified assumptions for the governing equations are the following:

- Viscous dissipation is negligible.
- External flow of moist air consists of two species (dry air and water vapor)
- Flow of moist air is considered as a mixture of ideal gas.
- Total derivative of pressure is negligible.
- There is no volumetric heat source.

Mass conservation is written as follows:

$$\frac{\partial \rho}{\partial t} + \mathrm{div}(\rho \mathbf{v}) = S_m$$

$$\rho = \sum_i \rho_i \; ; \quad i = a, v$$

$$\rho \mathbf{v} = \sum_i \rho_i \mathbf{v_i} \tag{1}$$

where ρ and $\mathbf{v}$ refer to the density of air and velocity (m s^{-1}), respectively, generally dependent on time t and location $\mathbf{x}$. Also, dry air and water vapor, respectively, noted a and v. S_m is source of mass in fluid due to evaporation of water from the apple sample.

The momentum conservation equation for the moist air is commonly described by:

$$\frac{\partial(\rho \mathbf{v})}{\partial t} + \mathrm{div}(\rho \mathbf{v} \otimes \mathbf{v} + p\mathbf{I}) = \mathrm{div}(\boldsymbol{\tau}^c) + \rho \mathbf{b} \tag{2}$$

p is thermodynamical pressure (Pa), $\mathrm{I} = \delta_{ij} e_k \otimes e_j$ - unity tensor, e_k (versor in one direction defined by subscript k) and v_k (scalar magnitude of vector $\mathbf{v}$), $\boldsymbol{\tau}^c = \boldsymbol{\tau} + \boldsymbol{D}$ - the viscous and diffusive flux of momentum (Pa), $\mathbf{b}$ - mass force of Earth gravity (m s^{-2})

The diffusion for each species is modelled according to Fick's law:

$$\rho_i(\mathbf{v}_i - \mathbf{v}) = -\rho D \, \mathrm{grad} \frac{\rho_i}{\rho} \; ; \quad i = a, v \tag{3}$$

The energy conservation equation is written in terms of specific energy $e = u + \frac{\mathbf{v}^2}{2}$ - sum of internal and kinetic energy. The energy equation is resumed to

$$\frac{\partial(\rho e)}{\partial t} + \mathrm{div}(\rho e \mathbf{v} + p\mathbf{v}) = \mathrm{div}(\boldsymbol{\tau}^c \mathbf{v} + \mathbf{q}_{fluid}^C) + \rho \mathbf{b} \cdot \mathbf{v} + S_e \tag{4}$$

where $\mathbf{q}_{fluid}^C = \mathbf{q} + \mathbf{q}^D = \sigma \mathrm{grad} T + D_q \mathrm{grad} c$ - total heat flux in the fluid, S_e is source of energy due to evaporation in fluid.

The heat flux $\mathbf{q}$ is expressed by the Fourier's law,

$$\mathbf{q} = -\sigma \mathrm{grad} T \tag{5}$$

σ is the thermal conductivity (Wm^{-1} K^{-1}).

The moisture conservation can be written as:

$$\frac{\partial c}{\partial t} + \mathrm{div}(c\mathbf{v}) = \mathrm{div}(D \mathrm{grad} c) + S_c \tag{6}$$

where grad$c$ represents the concentration gradient, D is the mass diffusivity and c is species concentration for mass transfer.

$S_c = S_m$ is the source of species in fluid due to evaporation of water from the apple.

After the first minute, the pressure in the chamber is not varied with respect to time and it remains constant at 20000 Pa. During this period, there is not any bulk flow and there is just the motion of vapor particles. The conservation equations of energy and species reduce to the following form respectively:

$$\frac{\partial(\rho e)}{\partial t} + \text{div}(p\mathbf{v}) = \text{div}\left(\boldsymbol{\tau}^c \mathbf{v} + \mathbf{q}_{fluid}^C\right) + \rho \mathbf{b} \cdot \mathbf{v} + S_e$$

$$\frac{\partial c}{\partial t} = \text{div}(D\text{grad}c) + S_c \tag{7}$$

2.2. Modelling for the porous medium (sample)

The sample is a square shape with 2 cm length considered as a porous body where is located in the center of the chamber (Figure 1). Initial temperature of the sample and moisture potential of air are, respectively, 30 °C and 87 (°M). The sample is considered as a solid body in the flow, so the velocity of all the nodes within the square material is equal to zero.

The following assumptions were used for modeling the heat and moisture transfer in the sample:

(1) Heat is transferred through conduction within the material.
(2) Mass is transferred inside the material through molecular diffusion.
(3) The dimension variation and deformation of the sample are negligible.
(4) Thermophysical properties of apple are dependent on temperature and moisture content.
(5) The air around the sample does not enter inside the apple.

The model due to Luikov is used for simultaneous modeling of heat and mass transfer in the sample (Luikov, 1975). A typical heat and mass transfer problem are governed by Luikov's equations, which related to drying a porous moist slab under constant pressure. The phase-change occurring within the slab act as heat source or sink resulting in the coupled relationship between mass transfer and heat transfer. In a coupled problem, the heat of absorption or desorption is generally one of the sources or sinks as well. This heat is not negligible for some hygrothermal materials. Luikov equations are written as follows, so that they are discussed more thoroughly in the Appendix A.

$$\rho c_q \frac{\partial T}{\partial t} = \text{div}\left[\left(k_q + \varepsilon\lambda k_m \delta\right)\text{grad}T + \varepsilon\lambda k_m\text{grad}\theta\right]$$

$$\rho c_m \frac{\partial \theta}{\partial t} = \text{div}[k_m \text{grad}\theta + k_m \delta \text{grad}T] \tag{8}$$

where θ is body moisture potential (^{0}M), c_q and c_m refer to the heat capacity (J.kg^{-1}.K^{-1}) and mass capacity (1.^{0}M^{-1}) respectively and k_q and k_m are thermal conductivity (W.m^{-1}.K^{-1}) and mass diffusivity (kg.m^{-1}.s^{-1}.^{0}M^{-1}) coefficient, respectively. ε is the penetration of the moisture vapor permeability coefficient, and λ is the latent heat of vaporization (J.kg^{-1}), δ is the coefficient of thermal gradient (K.m^{-1}) and T is the temperature (^{0}C).

The principles of invariable thermodynamics are used by Luikov to deduce the mentioned equations and nominated the concept of moisture potential to characterize the equivalence between heat and moisture potential. The moisture potentials of several bodies are equal to each another, if they are in thermodynamic equilibrium, although their specific moisture contents are not necessarily equal. The moisture potential (θ) is related to moisture content ($\emptyset$) by:

$$\emptyset_m = \left(\frac{\partial \emptyset}{\partial \theta}\right)_T \tag{9}$$

For a constant specific moisture capacity:

$$\emptyset = \emptyset_m . \theta \tag{10}$$

Moisture content in the heat and mass transfer equations is non-dimensionalised using the following equation (Karami, Kaveh, Mirzaee-Ghaleh, and Taghinezhad, 2018; Kaveh, Abbaspour-Gilandeh, and Nowacka, 2021; Zadhossein et al., 2021):

$$\text{Moisture Ratio (M.R)} = \frac{\emptyset - \emptyset_d}{\emptyset_0 - \emptyset_d} \tag{11}$$

Subscripts of d and 0 refers to dry and initial, respectively.
Thermo-physical properties of apple and dry conditions employed in the numerical simulation are listed in Table1.

Table 1 Thermo-physical properties of apple *(Nadi, Rahimi, Younsi, Tavakoli, And Hamidi-Esfahani, 2012)*

Properties and conditions	
Mass capacity, C_m	*0.01 (1.^{0}M^{-1})*
Heat capacity, C_q	4184 (0.05304+M) (j.kg^{-1}.k^{-1})
Mass conductivity coefficient, k_m	*2.2*10^{-8}(kg.m^{-1}.s^{-1}.^{0}M^{-1})*
Thermal conductivity coefficient, k_q	*0.0159M+0.0025T–0.994(*w.m^{-1}.k^{-1})
The ratio of the diffusion coefficient of vapor to diffusion of moisture, ε	0.3
the latent heat of vaporization, λ	2.5*10^6 (J.kg^{-1})
The coefficient of the thermal gradient, δ	2 (K.m^{-1})
Density, ρ	(exp (-0.66M) 0462.–0.852)1000 (kg.m^{-3})

3. Evaluation of numerical model

To solve the flow and heat and mass transfer by control volume method, the SIMPLE algorithm has been used. SIMPLE is an acronym for Semi-Implicit Method for Pressure Linked Equations. Velocity and pressure equations have been coupled in SIMPLE (Layeni et al., 2020). A portion of the two-dimensional grid used for the discretization is shown in Figure 2.
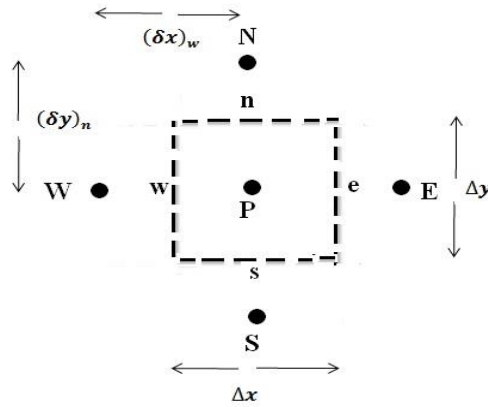

Figure 2. A part of the two-dimensional grids

Diffusion terms are discretized using the central differencing scheme and convection terms are discretized using the power-law scheme. In addition, the time term is also implicitly discrete. The general form of discretized equation in two-dimensional, laminar and unsteady flow for different schemes is as follows (Patankar and Spalding, 1983):

$$a_p\phi_p = a_e\phi_E + a_w\phi_W + a_n\phi_N + a_s\phi_S + b \tag{12}$$

Where coefficients are:

Table2. coefficients of the discretized equation

a_E	a_w	a_N	a_S
$D_eA(|Pe_e|) + [[-F_e, 0]]$	$D_wA(|Pe_w|) + [[F_w, 0]]$	$D_nA(|Pe_n|) + [[-F_n, 0]]$	$D_sA(|Pe_s|) + [[F_s, 0]]$

variables F_n, F_s, F_w, F_e and D_n, D_s, D_w, D_e represent the convective mass flux and diffusion conductance at cell faces, respectively (Patankar and Spalding, 1983). In the above relation function of $A(|Pe|)$ shows used scheme that is a function of the local Peclet (Table3):

Table3. Function of $A(|Pe|)$ for different schemes

$A(|Pe|)$	Scheme
$1 - |Pe|$	central differencing scheme
1	Upwind scheme
$[[1 - 0/5|Pe|\ , 0]]$	Hybrid scheme
$[[(1 - 0/1|Pe|)^5, 0]]$	Power-law scheme

In the implicit scheme for time, the source term has been linearized as $b = S_p \phi_p + S_u$.

$$a_p \phi_p = a_e \phi_E + a_w \phi_W + a_n \phi_N + a_s \phi_S + a_p^0 \phi_p^0 + S_u$$

$$a_p = a_p^0 + a_w + a_n + a_s + a_e - S_p \qquad (13)$$

The time marching procedure has been started with a given initial field of ϕ_p^0. The equation 13 has been solved after choosing time step dt. Next the solution ϕ_p is allocated to ϕ_p^0 and the procedure has been repeated to progress the solution by a subsequent time step. It can be illustrated that all coefficients are positive, which lead the implicit scheme to be unconditionally stable for each size of time step. To ensure the accuracy of the results, small time step is needed. The implicit scheme has been recommended for general goal transient calculations due to its robustness and unconditional stability.

The multi-generation and integrated energy system was significantly affirmed as a technology that aids the impressive use of energy source (Abam et al., 2020). The governing equations are integrated on the control volumes, in which case the governing differential equations will be replaced by a system of algebraic equations. Then, to solve such system of algebraic equations, the tri-diagonal matrix algorithm (TDMA) is used and the obtained equation is solved by the control volume method. Although the TDMA has been defined as a direct method for one dimensional situations, it can be exerted iteratively, in a line-by-line fashion, to solve multi-dimensional subjects and has been used in CFD programs. The grid used for conjugate modeling is integrated to avoid several district fragmentations within the domain. To this end, it was necessary to increase the number of edge nodes and borders nodes of the sample inside the chamber as shown in Figure 3.
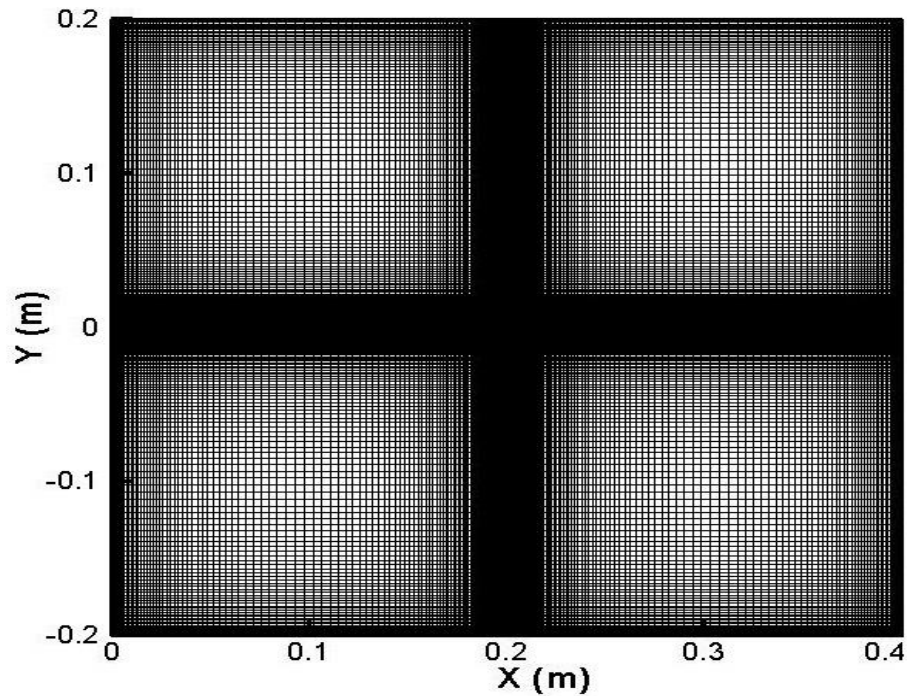
Figure 3. A grid of sample and chamber flow

3.1 Non-Use of boundary conditions

To avoid using empirical transfer coefficients, the vacuum drying has been simulated with non-use of boundary condition between porous sample and its surroundings. To achieve this purpose, coefficients and source terms for the borders of sample defined as follows.

Since the flow is in contact with the sample, the shear force in the x-direction is excreted on top and bottom surfaces while it is on the left and right surfaces in the y-direction. The top and bottom boundaries of the control volume are shown in Figure 4.
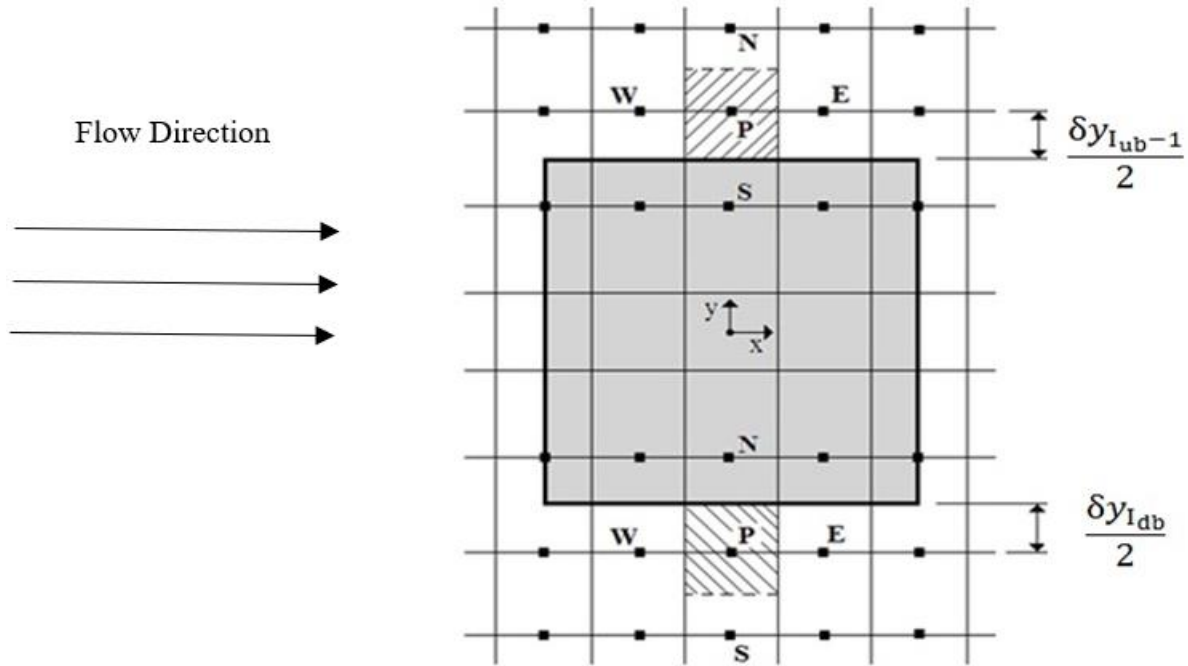
Figure 4. The control volume related to the shear stress on the top and bottom boundaries

The effect of this force enters the discretized equations as presented in the equations 14-17.

Shear stress on the upper border of the sample for the momentum equation along x reads:

$$F_{shear} = -\tau_{wall} \cdot A_{cell} = -2 \frac{\mu \cdot A_{cell}}{\delta y_{J_{ub}-1}} u_p$$

$$S_p = S_p - 2 \frac{\mu A_{cell}}{\delta y_{J_{ub}-1}}$$

$$a_s = 0 \tag{14}$$

Where $F_{shear}(N)$ is a shear force, $\tau_{wall}(N.m^{-2})$ is a shear stress, $A_{cell}\ (m^2)$ is the area of the sample, $\mu(kg.m^{-1}.s^{-1})$ dynamic viscosity, $u_p(m.s^{-1})$ flow velocity in the direction of central node, a_s is south coefficient of the discretized equation and Sp – the source term. The latter two quantities result from the definitions of the solving procedure described in detail in Patankar and Spalding (1983). Shear stress on the lower border of sample for the momentum equation along x is:

$$F_{shear} = -\tau_{wall} \cdot A_{cell} = -2 \frac{\mu \cdot A_{cell}}{\delta y_{J_{db}}} u_p$$

$$S_p = S_p - 2\frac{\mu \cdot A_{cell}}{\delta y_{J_{db}}}$$

$$a_n = 0 \tag{15}$$

Here, a_n is the north coefficient of the discretized equation.

Control volumes of shear stress on the upstream and downstream boundaries are illustrated in Figure 5.
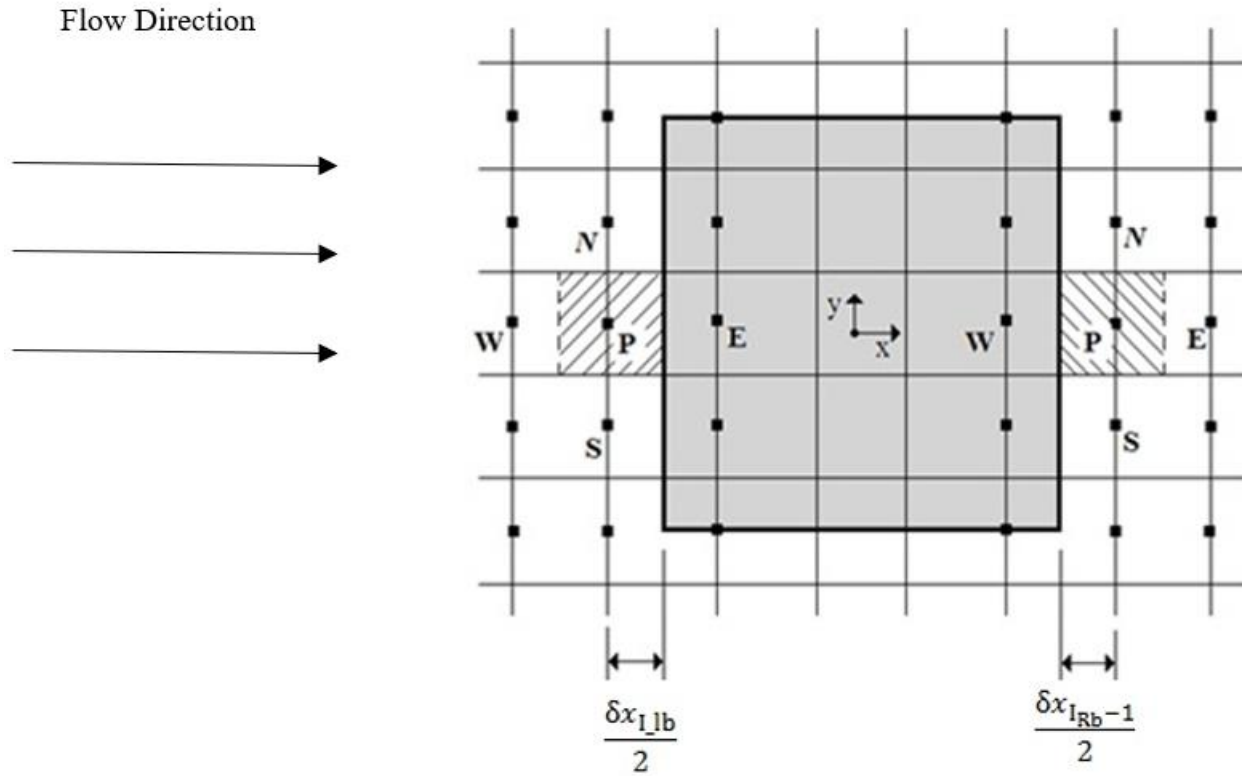

Figure 5. The control volume (upstream and downstream)

Shear stress on the downstream boundary of the sample for y momentum equation is defined as:

$$F_{shear} = -\tau_{wall} \cdot A_{cell} = -2\frac{\mu \cdot A_{cell}}{\delta x_{I_{Rb}-1}} v_p$$

$$S_p = S_p - 2\frac{\mu \cdot A_{cell}}{\delta x_{I_{Rb}-1}}$$

$$a_w = 0 \tag{16}$$

Where $v_p (m.s^{-1})$ is the velocity perpendicular to the direction of flow of central node and a_w is western coefficient of the discretized equation.

Shear stress on the upstream boundary of the sample for y momentum equation:

$$F_{shear} = -\tau_{wall} \cdot A_{cell} = -2\frac{\mu \cdot A_{cell}}{\delta x_{I_{lb}}} v_p$$

$$S_p = S_p - 2\frac{\mu \cdot A_{cell}}{\delta x_{I_{lb}}}$$

$$a_e = 0 \tag{17}$$

where $v_p (m.s^{-1})$ is the velocity perpendicular to the direction of flow of central node and a_e is the eastern coefficient of the discretized equation.

In order to peruse the effects of thermophysical parameters of sample and its surrounding on each other as an integrated domain, the sample and vacuum chamber are indicated in Figure 6. The left and right borders of sample are $I\_L(ii)$ and $I\_R(ii)$ respectively. As the same way, j_db and j_ub are specified as down and up border of sample.
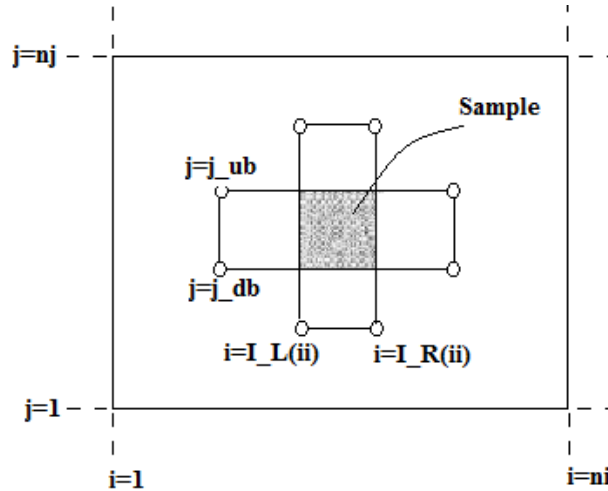
Figure 6. Sample and its borders

To consider sample and its environment as an integrated domain, the following parameters are defined.

$$k_s = k_q + \varepsilon\lambda k_m \delta \qquad From\ Eq.8$$

$$k_{eq} = 2 * \frac{k_s k_f}{k_s + k_f} \tag{18}$$

Where k_f is thermal conductivity coefficient of environment.

Diffusion conductance at left and right faces of sample are:

For $\quad$ $i = I\_L(ii)$ $\qquad$ $D_e = \dfrac{k_{eq}\Delta y}{(\delta x)_e}$

For $\quad$ $i = I\_R(ii)$ $\qquad$ $D_w = \dfrac{k_{eq}\Delta y}{(\delta x)_w}$

$$(19)$$

And for down and up faces of sample determine as follows:

For $\quad$ $j = j\_db$ $\qquad$ $D_s = \dfrac{k_{eq}\Delta x}{(\delta y)_s}$

For $\quad$ $j = j\_ub$ $\qquad$ $D_n = \dfrac{k_{eq}\Delta x}{(\delta y)_n}$

$$(20)$$

In order to moisture conservation, k_{m_eq} is defined as follows:

$$k_{m\_eq} = 2 * \frac{k_m D}{k_m + D} \qquad (21)$$

For moisture equations, diffusion conductance at left and right faces of sample are:

For $\quad$ $i = I\_L(ii)$ $\qquad$ $D_e = \dfrac{k_{m\_eq}\Delta y}{(\delta x)_e}$

For $\quad$ $i = I\_R(ii)$ $\qquad$ $D_w = \dfrac{k_{m\_eq}\Delta y}{(\delta x)_w}$

$$(22)$$

And for down and up faces of sample assess as follows:

For $\quad$ $j = j\_db$ $\qquad$ $D_s = \dfrac{k_{m\_eq}\Delta x}{(\delta y)_s}$

For $\quad$ $j = j\_ub$ $\qquad$ $D_n = \dfrac{k_{m\_eq}\Delta x}{(\delta y)_n}$

$$(23)$$

3.2 Grid Independence

Grid-independence leads to calculational results change along with a denser or looser grid that the truncation error can be ignored in numerical simulation. It should be noted that the grid

independence should be investigated in areas where the purpose of the simulation is to study them or they have a significant effect on the results. To achieve this, taking into account the mesh symmetry, the center of sample and for more confidence a point on the sample surface, for example the center of upper surface of sample are selected. So, to examine the independence of the results from the grid size, the variation of the humidity and temperature in the center of sample and the center of upper surface of sample versus time are shown in Figures 7 and 8 respectively. As it can be seen, the results of 109 × 109 grids are different from other grids. Even though the 152 × 152 and 234 × 234 consequences are approximately next to each other, the 344 × 344 consequence coincide with the 420 × 420 one and in order to lower computational cost, the 344 × 344 has been opted for.
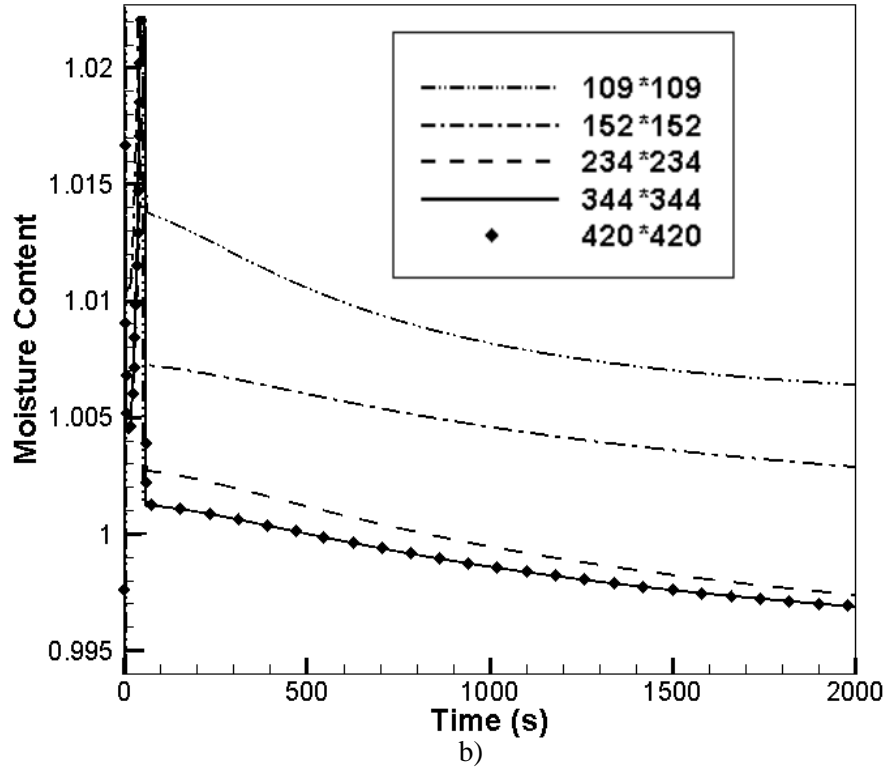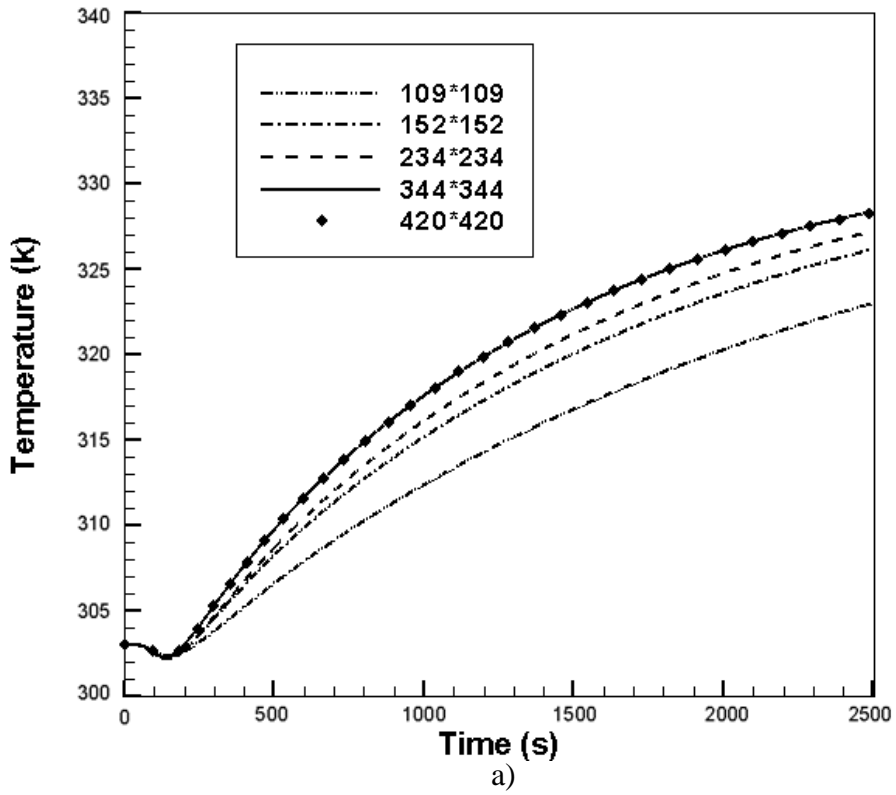

a)
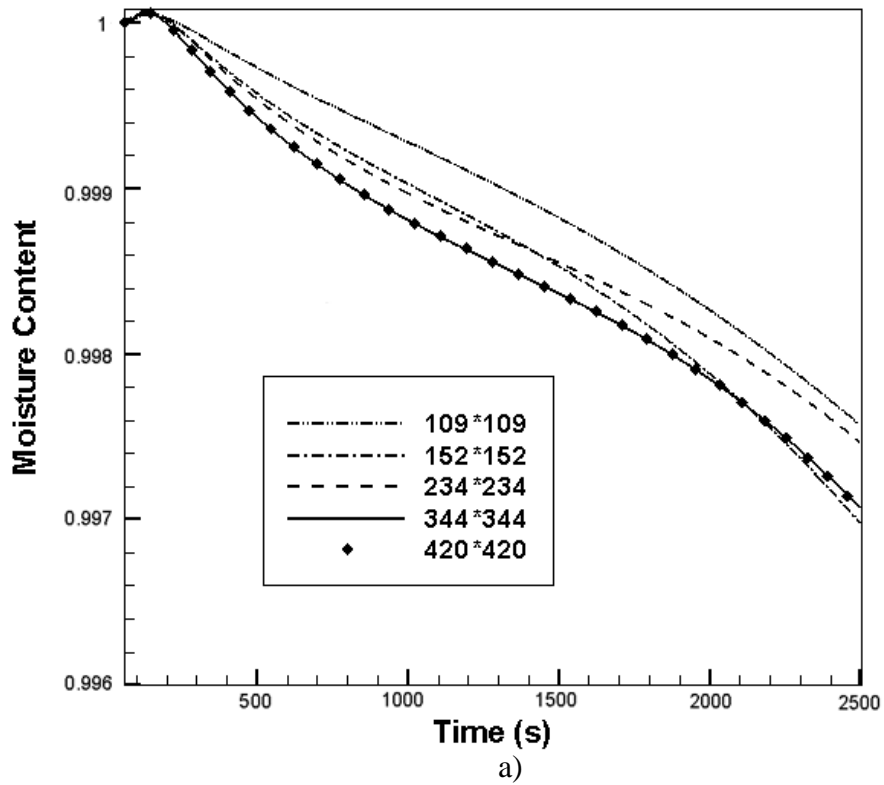
Figure **7.** The variation of humidity of a) sample center b) center of upper surface of sample versus time for different grids
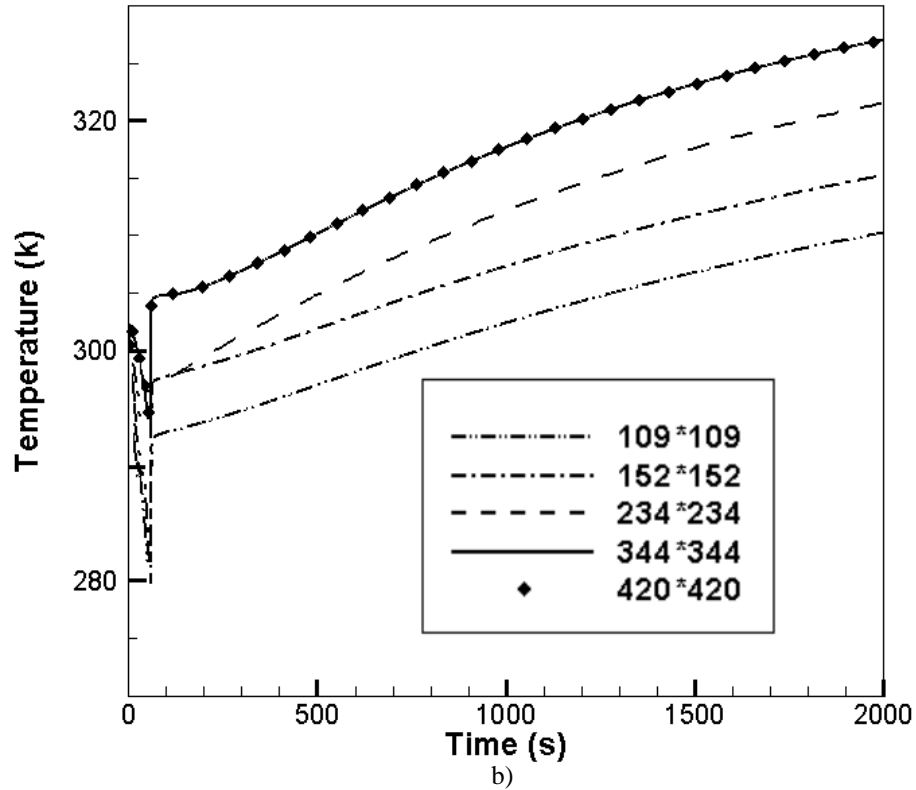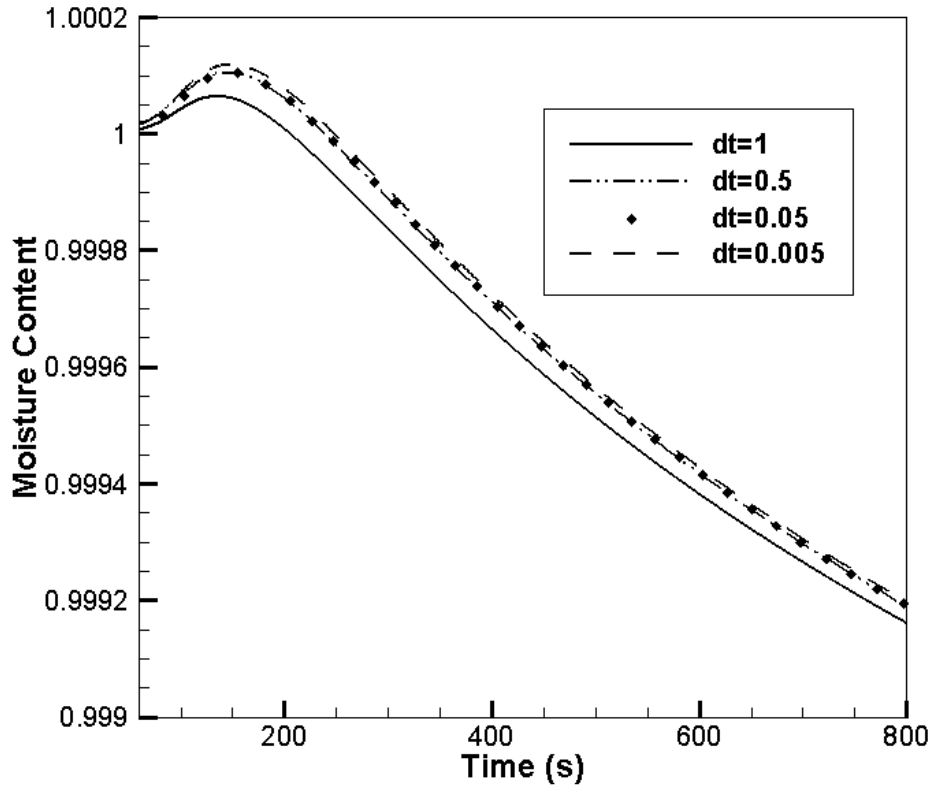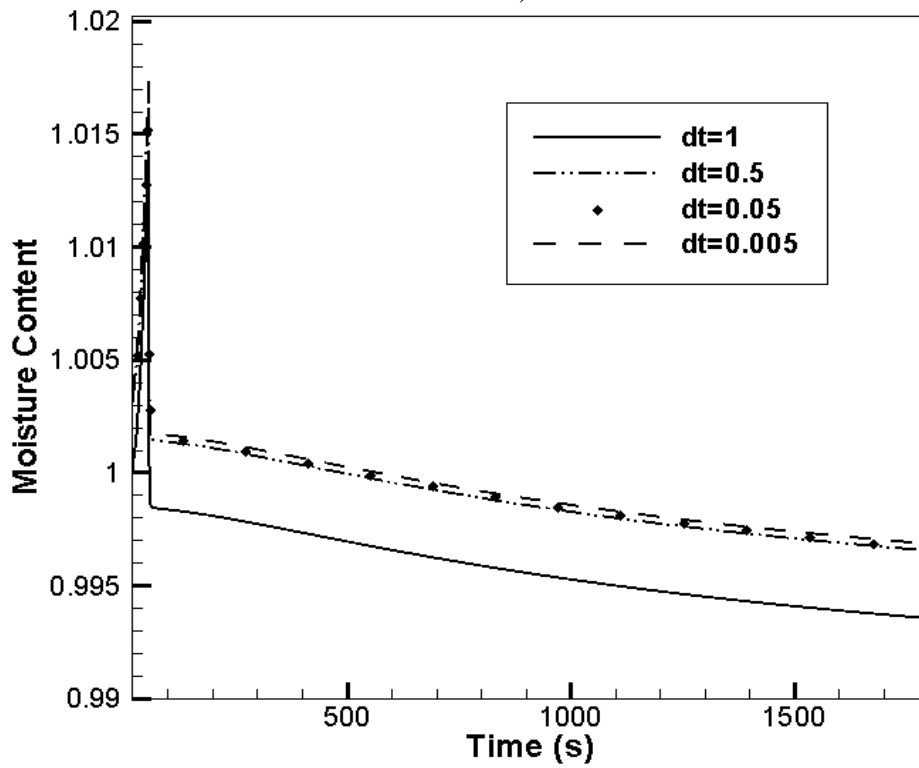
Figure 8. The variation of temperature of a) sample center b) center of upper surface of sample versus time for different grids

In order to assess the independence of results from time steps, the humidity and temperature of the center and the center of upper surface of sample which varies with respect time are shown for different time steps in Figures 9 and 10 respectively. These figures show that the suitable time step for this problem is equal 0.5 second.

a)

b)

Figure 9 The variation of humidity of a) sample center b) center of upper surface of sample versus time for different
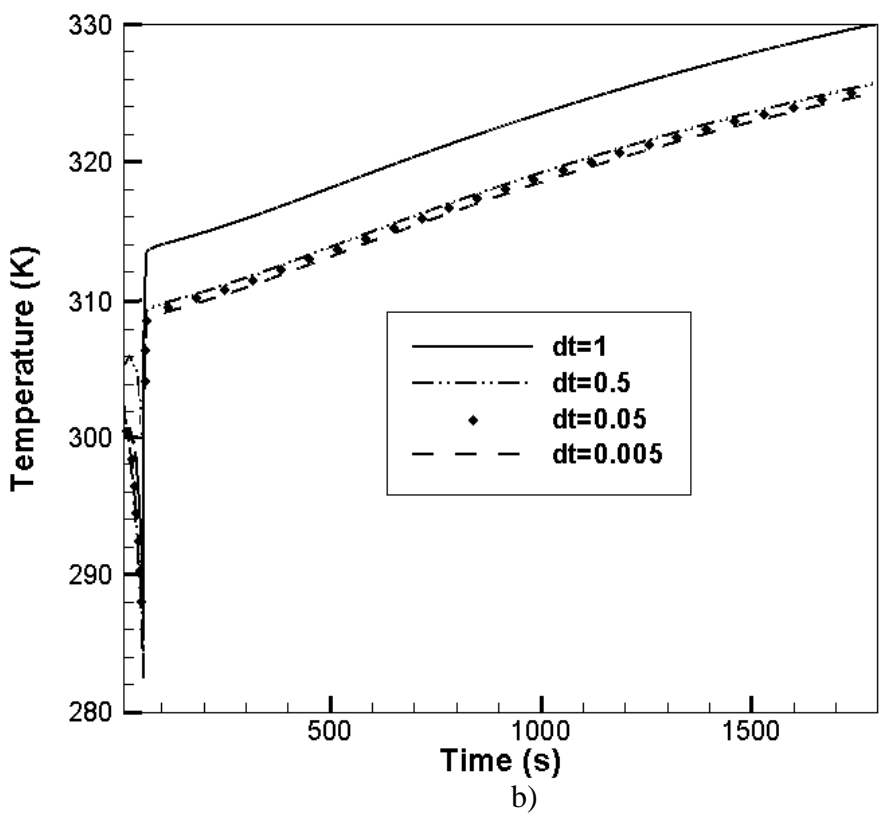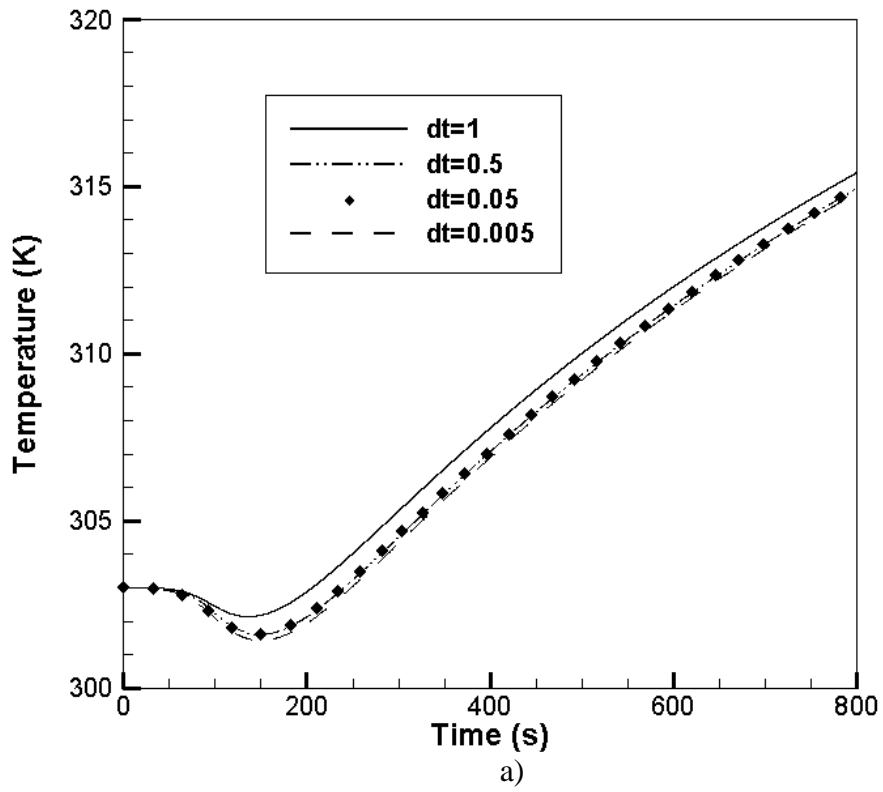time steps

Figure 10 The variation of temperature of a) sample center b) center of upper surface of sample versus time for different time steps

3.3 Model Validation

The predicted variation of the center temperature and moisture evolutions inside the rectangular object (apple) versus time were compared with the experimental data available in the literature (Figures 11a and 11b). Exceptionally good agreement was achieved between the experimental and the numerical results data taken from Chiang and Petersen (1987) and Hussain and Dincer (2003). The maximum difference between numerical results and experimental data was found to be less than 1% for the temperature and less than 0.82% for the moisture results. Therefore, it can be concluded that the present methodology is a proper tool for estimating temperature and moisture prediction of solid objects/products subjected to the vacuum drying.
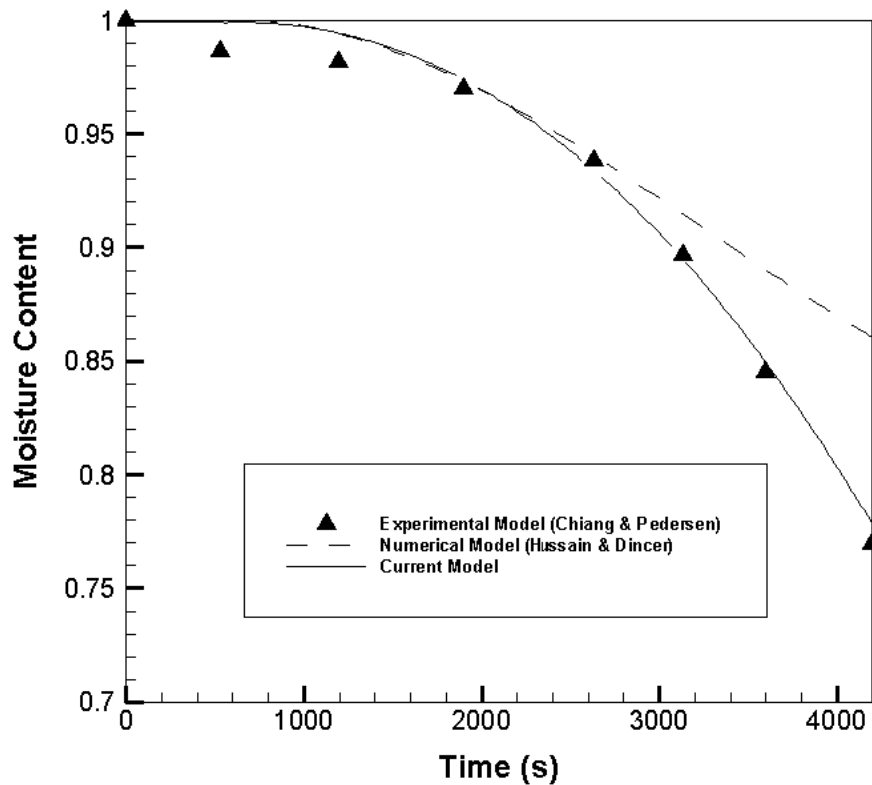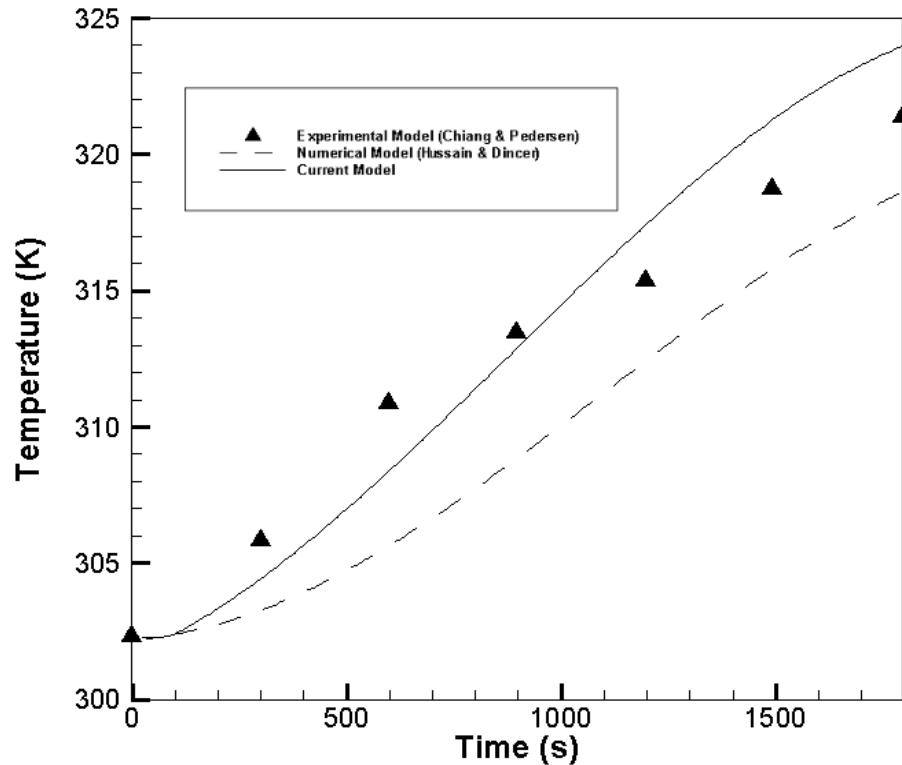
Figure 11. The comparison of experimental data (Chiang and Pedersen 1987), numerical (Hussain and Dincer 2003) and current numerical results (a) center moisture content and (b) The temperature for a square object (apple).

4. Results and discussion

The scrutinizing analysis is accomplished by dividing the drying operation into two periods. During the first one, pressure reduces linearly with respect to time till a value of 20 kPa is reached. Although this period seems to be negligible in duration, compared to the total drying time, Erriguible et al. show that this phase is characterized by important transport phenomena inside the product, so that neglecting it, would lead to substantial errors on the initial moisture, pressure and temperature fields. Humidity of chamber walls are constant just like their temperature. At the position of the pump, moisture content is assumed to be 50%. Iso-moisture contours in the chamber and the sample are shown in Figure 12 at the time of 50 second. As expected, the humidity inside the sample is transferred to its surfaces and added to the ambient air through evaporation due to the total pressure gradient. At the upper and right surfaces, the increase of moisture content of air can be explained by water transition of sample, so that pump location plays crucial role in regard to humidity transfer direction. Indeed, the sharp augmentation of moisture content implies strong gas pressure gradients giving rise to water transition towards the upper and right surfaces. As noted in Section 2.1, during first minute, drying is carried out by evaporation. In this case, the drying rate is a combination of convective and diffusive terms of vapor through humid air. Gas expansion in the vacuum chamber leads to decrease in gas density, while vapor mass fraction gradient

increases. Increasing discharge of gas from the sample results in gas velocity augments, whilst vapor density is fixed by the temperature and pressure conditions.
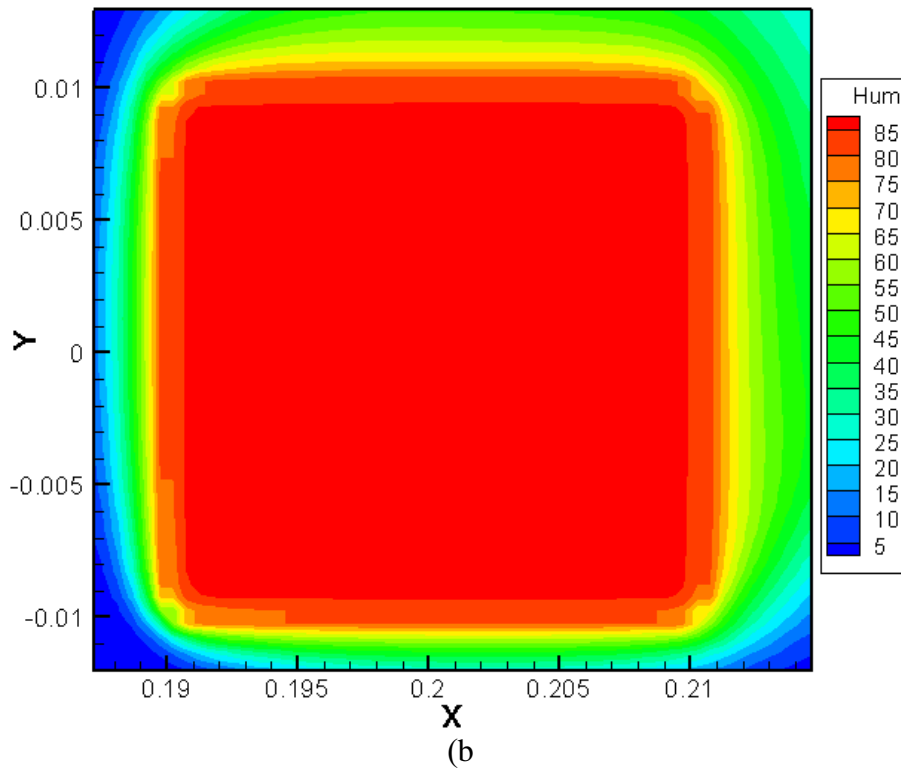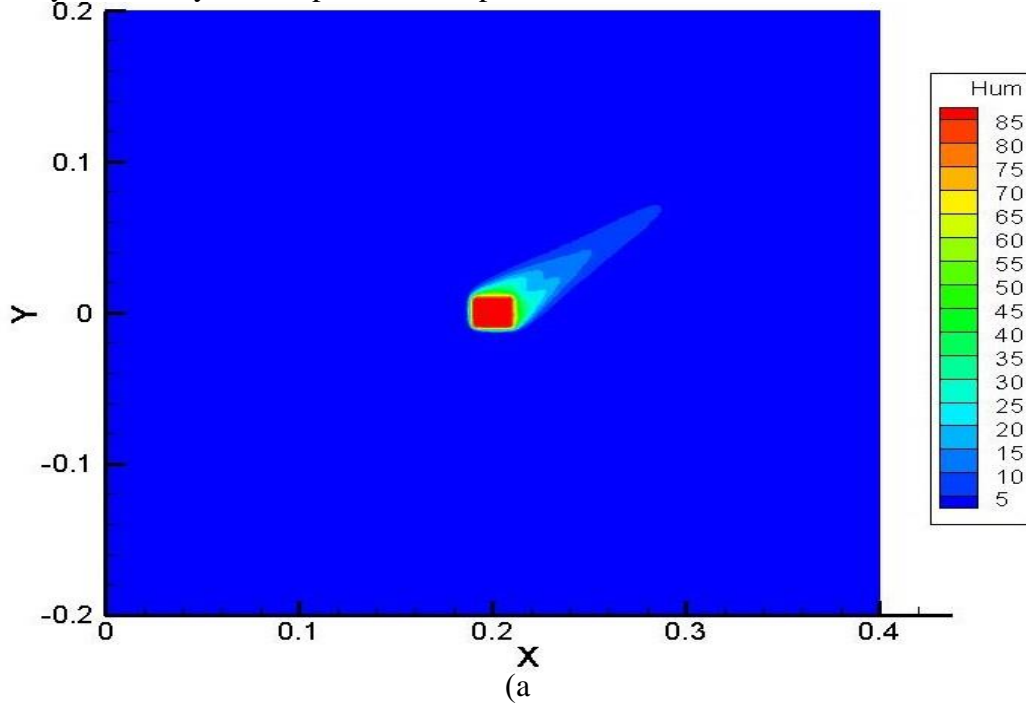

(a

(b

Figure 12. Iso-moisture contours a) in the vacuum chamber and b) inside the sample in 50 seconds

Iso-moisture contours in the vacuum chamber and the sample at the time of 200 seconds are shown in Figure 13. At this period, the gas pressure is not only low enough to reach its saturation value, but also dry air has been entirely removed from the sample. At every point in the sample, the water is conducted towards the top and right surface.
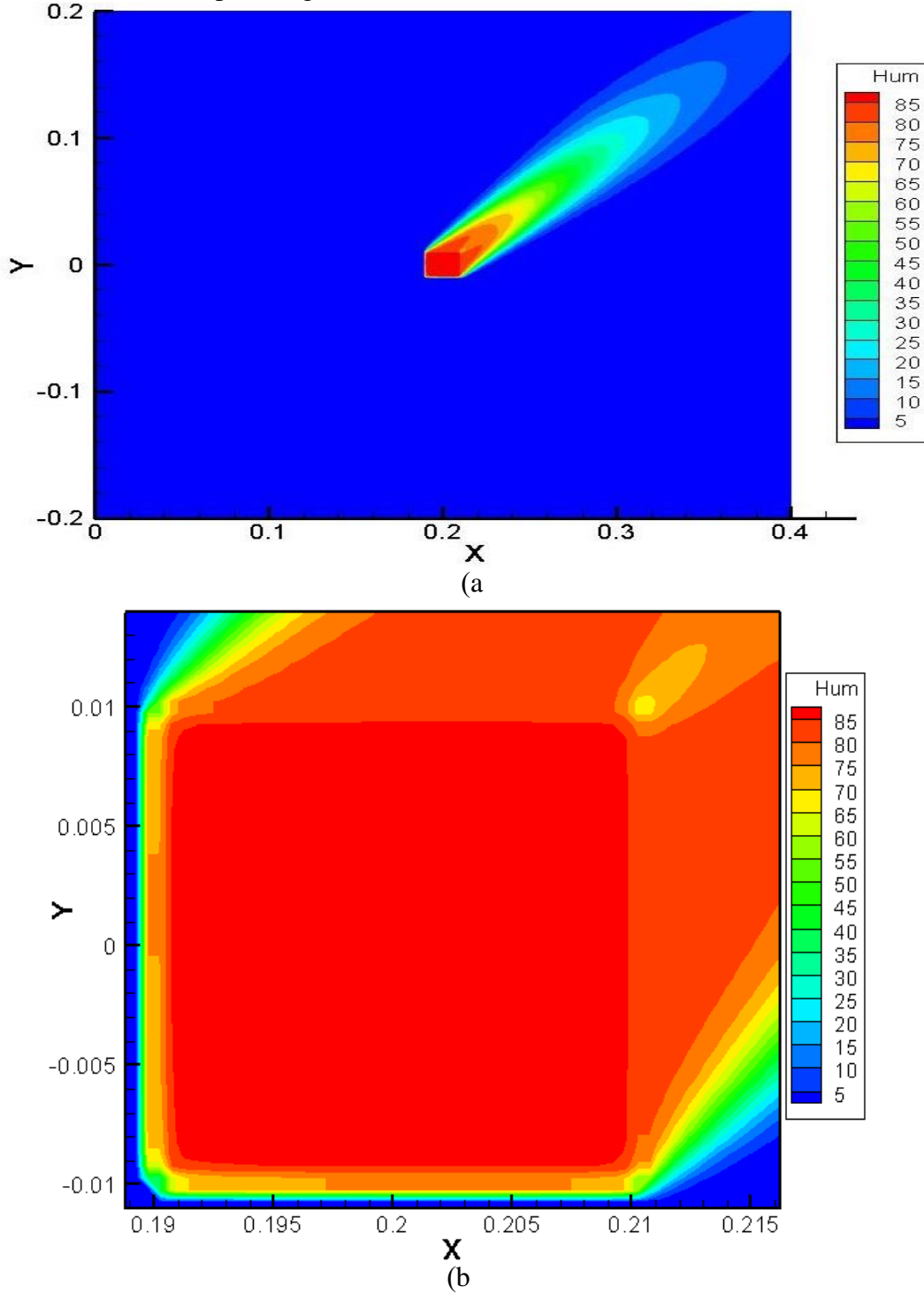

(a

(b

Figure 13. Iso-moisture contours a) in the vacuum chamber and b) inside the sample in 200 seconds

The moisture content in the center of the apple during drying processes is shown in Figure 14. This line chart represents what percentages of humidity transferred to apple surface across those times. According to the data given by this chart, it can be seen vividly that moisture content in the center of apple faced a falling trend. In the initial times, the rise of moisture content can be elucidated by water transfer owing to the total pressure gradient, then, decreasing of moisture content result from the substantial augmentation of total pressure. To more elaborate, water transfer dramatically to the apple surface due to strong gas pressure gradients.
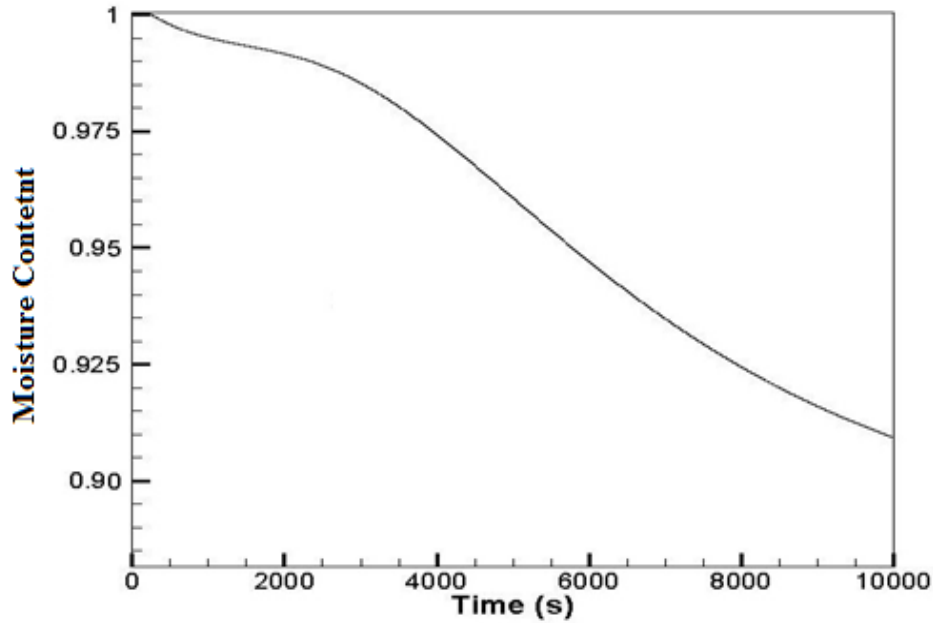

Figure 14. Evolution of moisture content at apple center during drying

The temperature in the center of the apple during drying processes is shown in Figure 15. Having studied the chart, it can be figured out that the temperature in the center of the apple faced a rising trend within those times. The temperature in the center of the apple after a slight reduction commenced to increase, and, then, remains constant at $333\ K$. The gas expansion in the chamber at first minute leads to reduce the temperature at apple surface since pressure is fixed by the pressure in the drying chamber. In other words, at the beginning of the drying process, the temperature reduces suddenly because water immediately evaporates from the apple due to abrupt pressure drop. The evaporated water removes heat from the slice in the form of the heat of vaporization; hence, the temperature drops. After this period, the temperature of the sample increases gradually until it reaches a constant value around the predeterminate medium temperature as expected. Then, it remains unchanged at this level until the surface of the sample starts to dry.
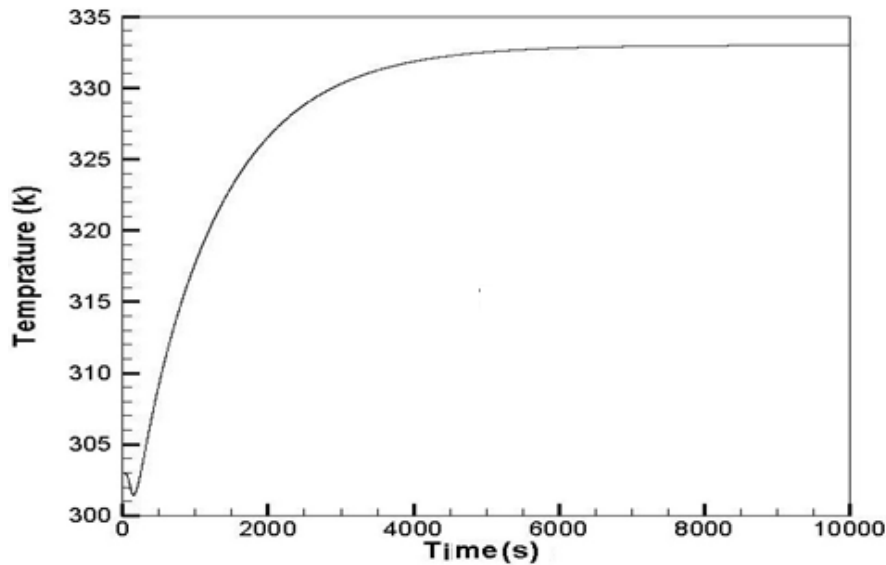
Figure 15. Evolution of temperature at apple center during drying

Figure16 represents isothermal and iso-moisture lines in the sample and its surroundings at 50, 100, 200 and 400 seconds. At first minute, moisture gradient between the apple surface and the bulk air has to be large enough. If the moisture content of air is very high and close to saturation, then the gradient will be low, and consequently the moisture cannot be eliminated. On the other hand, if the moisture content of air is low, the moisture elimination from the surface will be very slow. Hence the drying will take a longer time, which decreases the production capacity. In addition, the difference between the surface moisture content and that of the internal parts becomes large, which can cause shrinkage of apple. The moisture elimination rate from the surface plays an indispensable role on the drying process. When the air pressure decreases, the air density decreases. Decreasing the air density will lead to an increase in thermal diffusivity. This, in turn, causes the apple slice to reach the air temperature faster. Then, during the first minute, mass flow is more important due to the operation of the pump, so there is a pressure drop in the enclosure and consequently faster evaporation in the surface of the material. At 50 second, isothermal lines inside the sample are symmetric, so are the iso-moisture lines. As can be seen, the density of the isothermal and iso-moisture lines on the right and top of the sample surface are lower than other sides. It is indicating that the upward flow which is generated by pump result in decreasing the density of the Isothermal and Iso-moisture lines on the right and top of the sample surface. In order to understand the mechanism of heat and mass transfer inside the sample, Luikov considered the distribution of moisture in capillary-porous bodies to be either in the form of non-condensable air, vapor, liquid, or solid. The major difference between Luikov's model and the diffusion model is that in the former model the capillary forces are considered, and a differentiation between air, vapor, liquid, and solid is made. Luikov described the two phenomena associated with the transport of air, vapor and liquids through the porous media as molecular transport and molar transport. As the drying progresses at 100, 200 and 400 seconds, the temperature gradient in the surface region becomes high, which, in turn, accelerates conduction energy transport from the surface region to the solid bulk of the apple slice. So, as seen in the Figure 16 at 100,200 and 400 seconds, the distributions of isothermal and iso-moisture lines appear not to be symmetrical. Higher temperature and moisture gradients are obtained at the right and top of the sample surface.
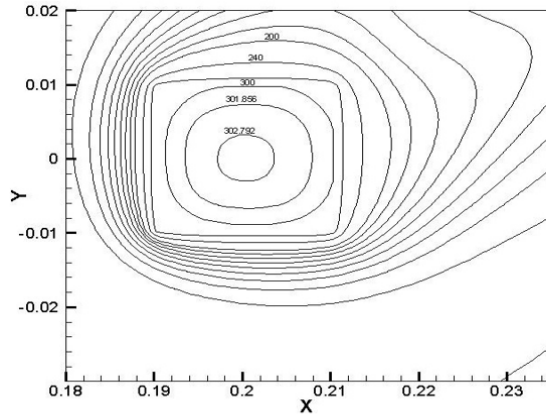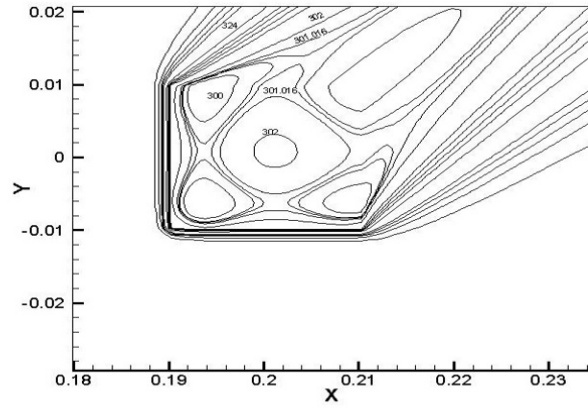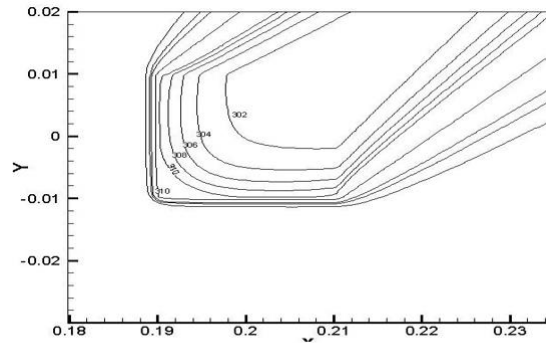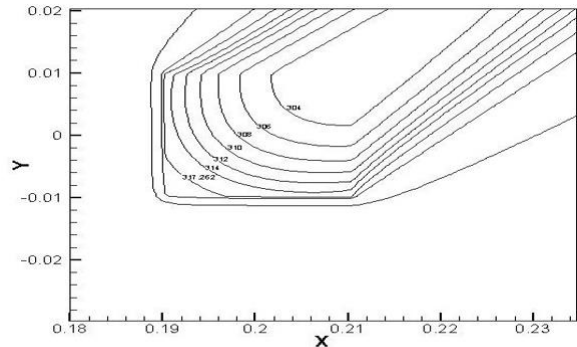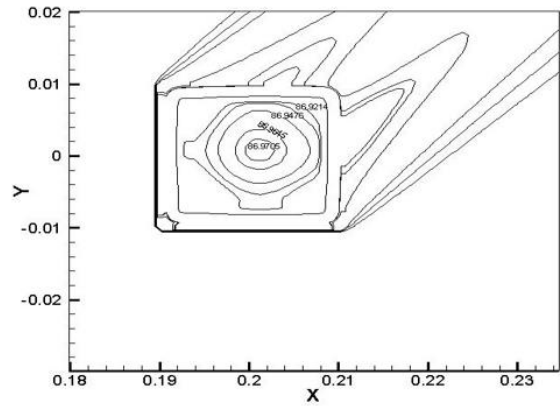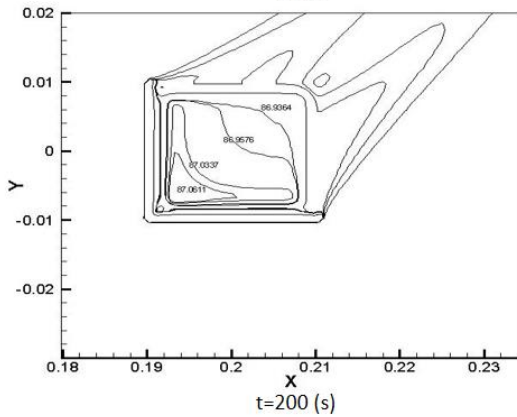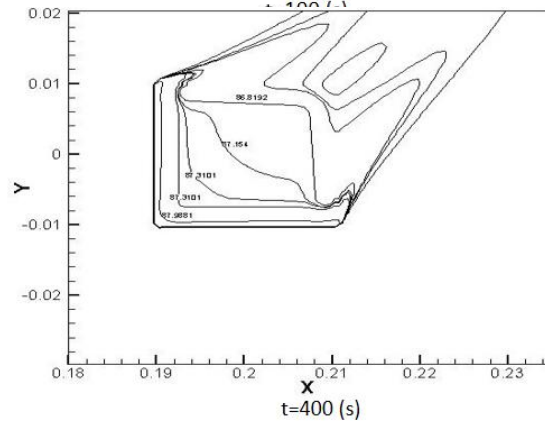
a) **Isothermal lines**
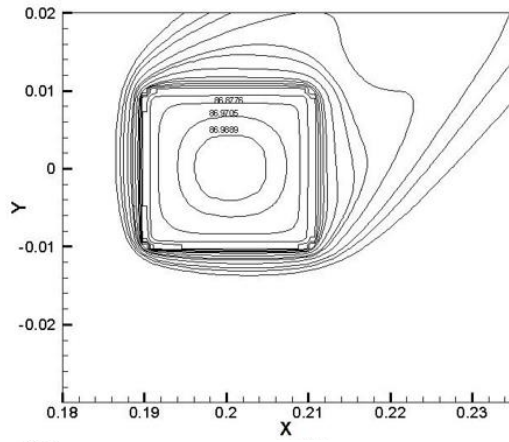

b) **Lines of constant moisture**

Figure 16. a) Isothermal, b) Iso-moisture lines in the sample and its surroundings for different time

5. Conclusion

In vacuum drying, the air of inside the chamber is sucked by a vacuum pump during one minute and subsequently in the second step, airflow is negligible and the fact that the relative fluid pressure inside the sample is higher than the chamber pressure causes to evaporate the water content of the sample. In this study, numerical solution for the distribution of temperature and humidity in the sample in a vacuum chamber was presented. Integrated solutions for the sample and the surrounding environment prevent disruption of solution area and there is no need for applying boundary conditions, mass and heat transfer coefficients around the sample. It was found that moisture content in the center of the apple faced a decreasing trend due to strong gas pressure gradients. In addition, the temperature in the center of the apple faced a rising trend. The drying process was conducted in two phases of variable pressure and constant pressure, where it was revealed that in the phase of gradual reduction of pressure, often neglected, the air flow was considered and it plays a significant role in the results. In this period, it is noticeable that high and low moisture content of air cannot result in removing moisture of the sample properly. Moreover, results showed that at the first minute, operation of pump and pressure drop in the chamber leads to faster evaporation of the sample. Results indicated the isothermal and iso-moisture lines inside and outside of the sample. Although at 50 second, isothermal and iso-moisture lines inside the sample are symmetric, they are not symmetric at 100, 200 and 400 second. At 50 second, density of the Isothermal and Iso-moisture lines on the left and bottom of the sample surface are more than other sides due to pump operation, but at 100, 200 and 400 second higher temperature and moisture gradients have been achieved at the right and top of the sample surface.

References:

Abam, Fidelis, Diemuodeke, Ogheneruona E, Ekwe, Ekwe, Alghassab, Mohammed, Samuel, Olusegun D, Khan, Zafar A, Imran, Muhammad, Farooq, Muhammad. (2020). Exergoeconomic and Environmental Modeling of Integrated Polygeneration Power Plant with Biomass-Based Syngas Supplemental Firing. *Energies, 13*(22), 6018.

Abbasi, Soleiman (2017). Yoghurt powder production using microwave–vacuum drier: drying kinetics, mathematical modeling, and characteristics. Journal of Food Science & Technology

Amiri, Milad, & Ayani, Mohammad Bagher. (2014). The Effect of Heat and Mass Transfer Coefficients on the Vacuum Drying of Porous Body, A Numerical Study. *Journal of Middle East Applied Science and Technology, 4*.

Andarwa, S, & Tabrizi, H Basirat. (2010). Non-Fourier effect in the presence of coupled heat and moisture transfer. *International Journal of Heat and Mass Transfer, 53*(15-16), 3080-3087.

Badur, Janusz, Feidt, Michel, & Ziółkowski, Paweł. (2020). Neoclassical Navier–Stokes Equations Considering the Gyftopoulos–Beretta Exposition of Thermodynamics. *Energies, 13*(7), 1656.

Boye, ThankGod E, & Samuel, Olusegun David. (2020). Computer-based method of design and modeling of transient flow in crude oil pipeline system. *Journal of Engineering Research, 8*(3).

Carullo, Alessio, & Vallan, Alberto. (2012). Measurement uncertainty issues in freeze-drying processes. *Measurement, 45*(7), 1706-1712.

Chang, Win-Jin, & Weng, Cheng-I. (2000). An analytical solution to coupled heat and moisture diffusion transfer in porous materials. *International Journal of Heat and Mass Transfer, 43*(19), .3621-3632

Chiang, Win-Chin, & Petersen, James N. (1987). Experimental measurement of temperature and moisture profiles during apple drying. *Drying Technology, 5*(1), 25-49.

Erriguible, A, Bernada, P, Couture, F, & Roques, M-A. (2007). Simulation of vacuum drying by coupling models. *Chemical Engineering and Processing: Process Intensification, 46*(12), 1274-1285.

Fohr, JP, Chakir, A, Arnaud, G, & Peuty, MA du. (1995). Vacuum drying of oak wood. *Drying Technology, 13*(8-9), 1675-1693.

Gawin, Dariusz, Pesavento, Francesco, & Schrefler, Bernhard A. (2006). Hygro-thermo-chemo-mechanical modelling of concrete at early ages and beyond. Part I: hydration and hygro-thermal phenomena. *International Journal for Numerical Methods in Engineering, 67*(3), 299-331.

Hussain, MM, & Dincer, I. (2003). Numerical simulation of two-dimensional heat and moisture transfer during drying of a rectangular object. *Numerical Heat Transfer: Part A: Applications, 43*(8), 867-878.

Incropera, Frank P, Lavine, Adrienne S, Bergman, Theodore L, & DeWitt, David P. (2007). *Fundamentals of heat and mass transfer*: Wiley.

Karami, Hamed, Kaveh, Mohammad, Mirzaee-Ghaleh, Esmaeil, & Taghinezhad, Ebrahim. (2018). Using PSO and GWO techniques for prediction some drying properties of tarragon (Artemisia dracunculus L.). *Journal of Food Process Engineering, 41*(8), e12921.

Karathanos, VT, & Saravacos, GD. (1993). Porosity and pore size distribution of starch materials. *Journal of food engineering, 18*(3), 259-280.

Kaveh, Mohammad, Abbaspour-Gilandeh, Yousef, & Nowacka, Malgorzata. (2021). Optimisation of microwave-rotary drying process and quality parameters of terebinth. *Biosystems Engineering, 208*, 113-130.

Kocaefe, Duygu, Younsi, Ramdane, Poncsak, Sandor, & Kocaefe, Yasar. (2007). Comparison of different models for the high-temperature heat-treatment of wood. *International Journal of Thermal Sciences, 46*(7), 707-716.

Kojic, M, Milosevic, M, Simic, V, Koay, EJ, Fleming, JB, Nizzero, S, . . . Ferrari, M. (2017). A composite smeared finite element for mass transport in capillary systems and biological tissue. *Computer Methods in Applied Mechanics and Engineering, 324*, 413-437.

Kostaropoulos, AE, & Saravacos, GD. (1995). Microwave pre-treatment for sun-dried raisins. *Journal of Food Science, 60*(2 .344-347 ,(

Layeni, Abayomi, Collins Nwaokocha, Olalekan Olamide, Giwa, Solomon, Tongo, Samuel, Onabanjo, Olawale, Samuel, Taiwo, . . . Samuel, Olusegun. (2020). Computational Analysis of a Lecture Room Ventilation System. *Zero-Energy Buildings: New Approaches and Technologies*, 77.

Luikov, Aleksei Vasilevič. (1975). Systems of differential equations of heat and mass transfer in capillary-porous bodies. *International Journal of Heat and Mass Transfer, 18*(1), 1-14.

Mohan, VP Chandra, & Talukdar, Prabal. .(2010)Three dimensional numerical modeling of simultaneous heat and moisture transfer in a moist object subjected to convective drying. *International Journal of Heat and Mass Transfer, 53*(21-22), 4638-4650.

Nalawade, Sagar A, Sinha, Akanksha, & Hebbar, H Umesh. (2018). Infrared based dry blanching and hybrid drying of bitter gourd slices: Process efficiency evaluation. *Journal of Food Process Engineering, 41*(4), e12672.

Nowacki, W. (1974). Dynamical problems of thermo diffusion in solids I.

Nummer, Brian A. (2002). Historical origins of food preservation. *National Center for Home Food Preservation. University of Illinois Extension*.

Onwude, Daniel I, Hashim, Norhashila, Abdan, Khalina, Janius, Rimfiel, & Chen, Guangnan. (2018). Investigating the influence of novel drying methods on sweet potato (Ipomoea batatas L.): Kinetics,

energy consumption, color, and microstructure. *Journal of Food Process Engineering, 41*(4), e12686.

Patankar, Suhas V, & Spalding, D Brian. (1983). A calculation procedure for heat, mass and momentum transfer in three-dimensional parabolic flows. In *Numerical prediction of flow, heat transfer, turbulence and combustion* (pp. 54-73): Elsevier.

Rani, Poonam, & Tripathy, PP. (2020). Modelling of moisture migration during convective drying of pineapple slice considering non-isotropic shrinkage and variable transport properties. *Journal of Food Science and Technology, 57*, 3748-3761.

Saravacos, GD. (1967). Effect of the drying method on the water sorption of dehydrated apple and potato. *Journal of Food Science, 32*(1), 81-84.

Shi, Ai-min, Li, Dong, Wang, Li-jun, Zhou, Yu-guang, & Adhikari, Benu. (2012). Spray drying of starch submicron particles prepared by high pressure homogenization and mini-emulsion cross-linking. *Journal of food engineering, 113*(3), 399-407.

Si, Xu, Chen, Qinqin, Bi, Jinfeng, Wu, Xinye, Yi, Jianyong, Zhou, Linyan, & Li, Zhaolu. (2016). Comparison of different drying methods on the physical properties, bioactive compounds and antioxidant activity of raspberry powders. *Journal of the Science of Food and Agriculture, 96*(6), 2055-2062.

Sontakke, Megha S, & Salve, Sanjay P. (2015). Solar drying technologies: A review. *International Journal of Engineering Science, 4*(4), 29-35.

Šumić, Zdravko, Tepić, Aleksandra, Vidović, Senka, Jokić, Stela, & Malbaša, Radomir. (2013). Optimization of frozen sour cherries vacuum drying process. *Food Chemistry, 136*(1), 55-63.

Sun, Dewei, Cao, Chen, Li, Bo, Chen, Hongjian, Cao, Peirang, Li, Jinwei, & Liu, Yuanfa. (2017). Study on combined heat pump drying with freeze-drying of Antarctic krill and its effects on the lipids. *Journal of Food Process Engineering, 40*(6), e12577.

Suvarnakuta, Peamsuk, Devahastin, Sakamon, & Mujumdar, Arun S. (2007). A mathematical model for low-pressure superheated steam drying of a biomaterial. *Chemical Engineering and Processing: Process Intensification, 46*(7), 675-683.

Swasdisevi, Thanit, Devahastin, Sakamon, Sa-Adchom, Poomjai, & Soponronnarit, Somchart. (2009). Mathematical modeling of combined far-infrared and vacuum drying banana slice. *Journal of food engineering, 92*(1), 100-106.

Wachowicz-Pyzik, Anna, Sowiżdżał, Anna, Pająk, Leszek, Ziółkowski, Paweł, & Badur, Janusz. (2020). Assessment of the Effective Variants Leading to Higher Efficiency for the Geothermal Doublet, Using Numerical Analysis–Case Study from Poland (Szczecin Trough). *Energies, 13*(9), 2174.

Yang, Haijian, Li, Yiteng, & Sun, Shuyu. (2020). Nonlinearly preconditioned constraint-preserving algorithms for subsurface three-phase flow with capillarity. *Computer Methods in Applied Mechanics and Engineering, 367*, 113140.

Yongsawatdigul, J, & Gunasekaran, S. (1996). Microwave-vacuum drying of cranberries: Part I. Energy use and efficiency. *Journal of Food Processing and Preservation, 20*(2), 121-143.

Younsi, R, Kocaefe, D, Poncsak, S, & Kocaefe, Y. (2007). Computational modelling of heat and mass transfer during the high-temperature heat treatment of wood. *Applied thermal engineering, 27*(8-9), 1424-1431.

Zadhossein, Safoura, Abbaspour-Gilandeh, Yousef, Kaveh, Mohammad, Szymanek, Mariusz, Khalife, Esmail, D Samuel, Olusegun, Amiri, Milad, Dziwulski, Jacek. (2021). Exergy and Energy Analyses of Microwave Dryer for Cantaloupe Slice and Prediction of Thermodynamic Parameters Using ANN and ANFIS Algorithms. *Energies, 14*(16), 4838.

Ziółkowski, Paweł, & Badur, Janusz. (2018). A theoretical, numerical and experimental verification of the Reynolds thermal transpiration law. *International Journal of Numerical Methods for Heat & Fluid Flow*.

Appendix A: Luikov equations

It is supposed a substance bounded and a capillary-porous sample. The bound substance is consisted of a liquid, vapor and inert gas at a positive temperature ($T > 0\,°C$), whereas it is included of ice, supercooled liquid (water), vapor and gas at a negative temperature ($T < 0\,°C$). The freezing temperature of water is changed over a wide range by energy of binding between the moisture and the sample. Therefore, at a negative temperature ($T < 0\,°C$), supercooled liquid is available in most cases in capillary-porous bodies. Another feature of mass transfer in capillary-porous bodies is that pores and body capillaries are filled by a gas and moisture (vapor, water, or ice). To more elaborate, water or ice and the remainder, with a vapor-gas mixture (humid air) fill a part of a capillary. A moist capillary-porous body is a multicomponent system including the bound substance ($k = 1,2,3,4$), so that it is defined steam like moisture (vapor), water, moisture in a solid state (ice) and inert gas (dry air) as $k = 1,2,3,4$, respectively. Meanwhile, $k = 0$ is allocated to dry body skeleton.

1. Differential Heat and Mass Transfer Equations

Molar and Molecular transport of vapor, water and air carry out simultaneously in a capillary-porous body. These types of transfer are conditionally named diffusion. Here, diffusion is defined as capillary diffusion (capillary absorption), molecular diffusion and convective diffusion (filtration). Density of a mass flow of the kth component of a bound substance in the state k ($k = 1,2,3,4$) is defined, so the differential mass transfer equation is:

$$\frac{\partial}{\partial t}(\rho_0 \emptyset_k) = -\text{div}\mathbf{j}_k + S_k \qquad (A.1)$$

Where t illustrates time, $\frac{\partial}{\partial t}()$ is derivative of variable with respect to time, S_k is the mass source or sink of the kth component, ρ_0 demonstrates density of moist body, $\emptyset_k$ represents the relative concentration of the bound body, $\mathbf{j}_k$ defines the density of a mass flow of the kth component of a bound substance in the state k ($k = 1,2,3,4$), the following differential equation is obtained:

$$\frac{\partial}{\partial t}(\rho_0 \emptyset) = -\sum_{k=1}^{4} \text{div}\mathbf{j}_k \qquad (A.2)$$

Sum of all the mass sinks and sources is zero:

$$\sum_{k=1}^{4} S_k = 0 \qquad (A.3)$$

The local derivative of the energy is equivalent to the divergence of an energy flow at constant pressure.

$$\frac{\partial}{\partial t}\left(e_0 \rho_0 + \sum_{k=1}^{4} \rho_0 \emptyset_k e_k\right) = -\text{div}\left(\mathbf{q} + \sum_{k=1}^{4} e_k \mathbf{j}_k\right) \qquad (A.4)$$

where $\mathbf{q}$ represents the heat flux, c_v is specific heat capacity at the constant volume, e illustrates the specific energy - $e = u + \frac{\mathbf{v}^2}{2}$ - sum of internal and kinetic energy, where $u = c_v T$ with T temperature.

The specific heat capacity at the constant pressure is designate through

$$c_{pk} = \frac{dh_k}{dT} \tag{A.5}$$

where $h_k = u_k + p_k v_k$ in which p_k represents thermodynamic pressure and v_k is specific volume, then:

$$\left(c_0\rho_0 + \sum_{k=1}^{4} \rho_0 \emptyset_k c_{pk}\right)\frac{\partial}{\partial t}T + \sum_{k=1}^{4} h_k \frac{\partial(\rho_0\emptyset_k)}{\partial t} = -\mathrm{div}\mathbf{q} - \sum_{k=1}^{4} c_{pk}\mathbf{j}_k \cdot \mathrm{grad}T - \sum_{k=1}^{4} h_k \mathrm{div}\mathbf{j}_k \tag{A.6}$$

where: $\frac{\partial}{\partial t}T = \frac{\partial T}{\partial t}$. Multiply Eq. (A.1) by h_k and sum up over $k = 1,2,3,4$

$$\sum_{k=1}^{4} h_k \frac{\partial(\rho_0\emptyset_k)}{\partial t} = -\sum_{k=1}^{4} h_k \cdot \mathrm{div}\mathbf{j}_k + \sum_{k=1}^{4} h_k S_k \tag{A.7}$$

From Eqs. (A.5) and (A.6) the differential heat transfer equation is obtained:

$$c\rho_0 \frac{\partial T}{\partial t} = -\mathrm{div}\mathbf{q} - \sum_{k=1}^{4} h_k S_k - \sum_{k=1}^{4} c_{pk}\mathbf{j}_k \cdot \mathrm{grad}T \tag{A.8}$$

where c represents the total specific heat capacity of a body

$$c = c_0 + \sum_{k=1}^{4} c_{pk}\emptyset_k \tag{A.9}$$

where c_0 illustrated the total specific heat capacity. From Eq. (A.7) for a moving liquid, the Fourier-Kirchhoff equation is obtained as a particular case. It is assumed $k = 2$

$$c\rho_0 = c_{p2}\rho_0\emptyset_2 = c_{p2}\rho_2 \qquad ; \ \mathbf{j}_2 = \rho_2\boldsymbol{\omega} \tag{A.10}$$

where $\boldsymbol{\omega}$ indicates concentration.

$$c_{p2}\rho_2 \frac{\partial T}{\partial t} + c_{p2}\rho_2\boldsymbol{\omega} \cdot \mathrm{grad}T = -\mathrm{div}\mathbf{q} \tag{A.11}$$

In capillary-porous bodies the convective component of heat transfer is small in comparison to the conductive one in the absence of filtration. So, the term $\sum_{k=1}^{4} c_{pk}\mathbf{j}_k \cdot \mathrm{grad}T$ is negligible. It is assumed that there are no chemical conversions in order to the formation of a noncondensing gas (dry air), so the source S_4 is considered zero ($S_4 = 0$).

Differential Eq. (A.7) is redacted as follows:

$$c\rho_0 \frac{\partial T}{\partial t} = -\mathrm{div}\mathbf{q} - \sum_{k=1}^{3} h_k S_k \tag{A.12}$$

Equations (A.1) and (A.12) illustrate a system of differential equations for heat and mass transfer with sources of mass S_k and heat $h_k S_k$, so that they are determined by phase conversion. In next sections, sources S_k and fluxes of heat and mass will be obtained.

A. The Mass Sources.

For $T > 0\ °C$, it is composed of two phases (liquid and vapor). From equation (A.3):

$$S_2 = -S_1 \tag{A.13}$$

Since the mass of vapor in capillaries is negligibly small in comparison to that of liquid ($\emptyset_2 >> \emptyset_1$), it is assumed that $\emptyset_1 = 0$. So, from Eq.A1:

$$\frac{\partial}{\partial t}(\rho_0 \emptyset_1) = -\text{div}\mathbf{j}_1 + S_1 = 0 \tag{A.14}$$

Hence the explanation for a liquid source is

$$S_2 = -S_1 = \text{div}\mathbf{j}_1\, div j_1 \tag{A.15}$$

At a temperature of the body $T > 0\ °C$, the same relation is obtained for the source. Changes in the mas of the liquid result from transfer $(d_0 \emptyset_2)$ and phase conversion $d_1 \emptyset_2$ i.e.,

$$d\emptyset_2 = d_0 \emptyset_2 + d_1 \emptyset_2 \tag{A.16}$$

Define relation $\frac{d_1 \emptyset_2}{d_0 \emptyset_2}$ through

$$\beta_2 = \frac{d_1 \emptyset_2}{d_0 \emptyset_2} \tag{A.17}$$

When no phase conversions occur $(d_1 \emptyset_2)$, $\beta = 0$ is obtained, and, when phase conversion ($d_0 \emptyset_2 = 0$) leads to all the changes of mass, $\beta = \infty$ is achieved. Therefore, ε_2 is defined as follows:

$$\varepsilon_2 = \frac{\beta_2}{1 + \beta_2} \tag{A.18}$$

Consequently, a diffusion equation of mass transfer will be obtained as:

$$\rho_0 \frac{\partial \emptyset_2}{\partial t} = -\text{div}\mathbf{j}_2 + \varepsilon_2 \rho_0 \frac{\partial \emptyset_2}{\partial t} \tag{A.19}$$

For ($\emptyset_2 = \emptyset$ for $T > 0\ °C$), comparing Eq. (A.19) with (A.1), below equation will be achieved:

$$S_2 = \varepsilon_2 \rho_0 \frac{\partial \emptyset_2}{\partial t} = \varepsilon_2 \rho_0 \frac{\partial \emptyset}{\partial t} \tag{A.20}$$

Allowing for $\partial \emptyset_1 / \partial t = 0$, it follows from Eqs. (A.1) and (A.2) at $T > 0\ °C$, that

$$S_2 = -S_1 = \varepsilon_2 \rho_0 \frac{\partial \emptyset}{\partial t} = -\text{div}\mathbf{j}_1 = -\varepsilon_2 (\text{div}\mathbf{j}_1 + \text{div}\mathbf{j}_2) \tag{A.21}$$

Where,

$$\varepsilon_2 = \frac{\text{div}\mathbf{j}_1}{\text{div}\mathbf{j}_1 + \text{div}\mathbf{j}_2} \tag{A.22}$$

Consequently, the amount of vapor transferred in a body in order to the whole vapor and liquid flow is defined by coefficient ε_2.

B. Calculation of Heat and Mass Flows

Molecular transport transfers vapor in the interior of a capillary-porous body. It is in thermodynamic equilibrium with liquid. A mass flow of vapor defines as follows:

$$\mathbf{j}_1 = -\varepsilon\rho D \text{grad}\rho_{10} = -a_{m1}\rho_0 \text{grad}\emptyset - a_{m1}^T \rho_0 \text{grad}T \tag{A.23}$$

Where ε represents a dimensionless factor characterizing resistance to vapor diffusion in a moist body. The vapor diffusion coefficient of a moist porous body is specified:

$$a_{m1} = \varepsilon D \frac{\rho}{\rho_0} (\frac{\partial\rho_{10}}{\partial\emptyset})_T \tag{A.24}$$

And thermal diffusion coefficient a_{m1}^T of a moist body is determined:

$$a_{m1}^T = \varepsilon D \frac{\rho}{\rho_0} (\frac{\partial\rho_{10}}{\partial T})_\emptyset \tag{A.25}$$

The liquid transfer in a capillary-porous body is characterized in an analogous manner, as functions of moisture content $\emptyset$ and body temperature T. It is obtained:

$$\mathbf{j}_2 = -a_{m2}\rho_0 \text{grad}\emptyset - a_{m2}^T \rho_0 \text{grad}T \tag{A.26}$$

Although the diffusion coefficient a_{m2} and the thermal diffusion coefficient a_{m2}^T of liquid in a porous body are not constant, depend on temperature and moisture content of the body. The heat flux according to Fourier's law is

$$\mathbf{q} = -k\text{grad}T \tag{A.27}$$

The coefficient of heat conduction k of a moist body depends on both $\emptyset$ and T.

According to equations (A.23), (A.26) and (A.27):

$$\frac{\partial\emptyset}{\partial t} = \text{div}[a_m(\text{grad}\emptyset + \delta\text{grad}T)] \tag{A.28}$$

$$c\rho_0 \frac{\partial T}{\partial t} = \text{div}(k \text{grad} T) + L\varepsilon\rho_0 \frac{\partial \emptyset}{\partial t} \tag{A.29}$$

Where L indicates a specific heat of phase transition, a_m represents a total moisture diffusion coefficient $a_m = a_{m1} + a_{m2}$; δ is a thermal gradient coefficient as follows

$$\delta = \frac{a_{m1}^T + a_{m2}^T}{a_{m1} + a_{m2}} \tag{A.30}$$

Where a_{m1} and a_{m1}^T are the diffusion coefficient and the thermal diffusion coefficient of a moist porous body are not constant, Then accounting to relations (A.15) and (A.20), Eqs (28) and (29) are defined as:

$$\frac{\partial \emptyset}{\partial t} = k_{11} \text{lap} \emptyset + k_{12} \text{lap} T \tag{A.31}$$

$$\frac{\partial T}{\partial t} = k_{21} \text{lap} \emptyset + k_{22} \text{lap} T \tag{A.32}$$

Where the transfer coefficients (k, $i = 1,2$) are

$$k_{11} = a_m = a_{m1} + a_{m2} \qquad ; \qquad k_{12} = a_m \delta = a_{m1}^T + a_{m2}^T$$

$$k_{21} = \frac{L\varepsilon}{c} a_m \qquad ; \qquad k_{22} = a + \frac{L\varepsilon}{c} a_m \delta$$

$$\tag{A.33}$$

C. Heat and Mass Transfer with Filtration

At intense heating of a moist body above 100°C there emerges a pressure gradient owing to liquid evaporation. Effusion of the humid air through micro-capillaries inside a body leads to a pressure gradient (grad $p \neq 0$) at temperature less than 100°C. The presence of inside a capillary-porous body result in filtration of vapor and liquid. This mode of transfer is defined by the Darcy law:

$$\mathbf{j}_f = -k_{fc} \text{grad} \, p \tag{A.34}$$

Where k_{fc} is the total filtration-coefficient.

In this case the system of differential equations for heat and mass transfer in a capillary-porous body is described as follows:

$$\frac{\partial \emptyset}{\partial t} = k_{11} \text{lap} \emptyset + k_{12} \text{lap} T + k_{13} \text{lap} p \tag{A.35}$$

$$\frac{\partial T}{\partial t} = k_{21} \text{lap} \emptyset + k_{22} \text{lap} T + k_{23} \text{lap} p \tag{A.36}$$

$$\frac{\partial p}{\partial t} = k_{31}\text{lap}\emptyset + k_{32}\text{lap}T + k_{33}\text{lap}p \qquad\qquad (A.37)$$

where coefficients are:

$$k_{13} = a_m\delta_f \qquad ; \qquad k_{23} = \varepsilon L\frac{a_m}{c}\delta_p \qquad ; \qquad k_{33} = a_f - \varepsilon\frac{a_m}{c_f}\delta_p$$

$$k_{31} = \frac{-\varepsilon a_m}{c_f} \qquad ; \qquad k_{32} = \frac{-\varepsilon a_m\delta}{c_f}\delta \qquad ; \qquad a_f = \frac{k_{fc}}{c_{fp}}$$

$$\delta_f = \frac{k_{fc}}{a_m\rho_0} \qquad\qquad\qquad\qquad (A.38)$$

Where a_f represents the coefficient of filtration diffusion, C_f is the body capacity for the humid air with filtration.

If it is assumed that the mass transfer inside the sample is considered liquid and at the surface of the sample is vapor, the governing equations of Luikov are as follows:

$$\rho c_q\frac{\partial T}{\partial t} = \text{div}\left[\left(k_q + \varepsilon\lambda k_m\delta\right)\text{grad}T + \varepsilon\lambda k_m\text{grad}\theta\right] \qquad\qquad (A.39)$$

$$\rho c_m\frac{\partial \theta}{\partial t} = \text{div}[k_m\text{grad}\theta + k_m\delta\text{grad}T]$$

$$(A.40)$$

Where θ represents body moisture potential (^{0}M), c_q and c_m illustrate the heat capacity (J.kg^{-1}.K^{-1}) and mass capacity (1.^{0}M^{-1}) respectively and k_q and k_m are thermal conductivity (W.m^{-1}.K^{-1}) and mass diffusivity (kg.m^{-1}.s^{-1}.^{0}M^{-1}) coefficient, respectively. ε indicate the penetration of the moisture vapor permeability coefficient, and λ is the latent heat of vaporization (J.kg^{-1}), δ is the coefficient of thermal gradient (K.m^{-1}) and T is the temperature ($^\circ$C).

The maximum moisture content of the reference body ($\emptyset_{sm}$) is achieved in the process of absorbing water vapor, which is defined as 100 degrees of mass transfer. Body moisture potential is considered by the reference body moisture content ($\emptyset_s$):

$$\theta = \frac{\emptyset_s}{\emptyset_{sm}}.100^\circ M \qquad\qquad (A.41)$$

$$\emptyset_m = (\frac{\partial\emptyset}{\partial\theta})_T \qquad\qquad (A.42)$$